ELSEVIER

Contents lists available at ScienceDirect

New BIOTECHNOLOGY

journal homepage: www.elsevier.com/locate/nbt



Catalytic versatility of lipoxygenase from Microcystis aeruginosa

Ruth Chrisnasari ^{a,b,c}, Shuyue Chen ^a, Roelant Hilgers ^a, Daan van Vliet ^b, Willem J.H. van Berkel ^a, Jean-Paul Vincken ^a, Tom A. Ewing ^b, Marie Hennebelle ^{a,*}

- ^a Laboratory of Food Chemistry, Wageningen University & Research, Bornse Weilanden 9, Wageningen 6708 WG, the Netherlands
- b Wageningen Food & Biobased Research, Wageningen University & Research, Bornse Weilanden 9, Wageningen 6708 WG, the Netherlands
- ^c Faculty of Biotechnology, University of Surabaya (UBAYA), Surabaya 60293, Indonesia

ARTICLE INFO

Keywords: Double dioxygenation Dihydroperoxide Epoxy alcohol Fatty acid oxidation Hydroperoxide Hydroperoxide isomerase Ketone

ABSTRACT

Lipoxygenases (LOXs) catalyze the regio- and enantioselective addition of molecular oxygen to polyunsaturated fatty acids (PUFAs), yielding fatty acid hydroperoxides (FAHPs) with significant industrial relevance. Bacterial LOXs are of particular interest due to their broad substrate range and distinct regio- and enantioselectivity profiles. In the current study, we characterized the biochemical properties and product scope of a newly identified LOX from the cyanobacterium Microcystis aeruginosa (Ma-LOX). Our results demonstrate that Ma-LOX exhibits a strong preference for linoleic acid (LA) and α-linolenic acid (ALA), catalyzing regioselective dioxygen insertion predominantly at the ω-5 position for these substrates. Notably, this regioselectivity diminishes with longer-chain PUFAs. Ma-LOX shows opposite enantioselectivity with respect to eukaryotic LOXs, producing 13(R)-hydroperoxy-9Z,11E-octadecadienoic acid (13R-HPODE) from LA with an enantiomeric excess (ee) of $79.3 \pm 8.8 \%$ (n = 3). Structural prediction and molecular docking simulations suggest that the observed regioselectivities of Ma-LOX are influenced by oxygen insertion via two distinct pathways: a putative oxygen access channel and the entrance of a relatively shallow substrate-binding pocket, distinguishing Ma-LOX from other LOXs. Additionally, we identified that this shallow binding pocket facilitates Ma-LOX's double dioxygenation activity toward ALA, resulting in the formation of dihydroperoxides. Beyond FAHPs and dihydroperoxides, Ma-LOX catalyzes the synthesis of epoxy alcohols and ketones, suggesting the enzyme possesses an unusual but highly relevant hydroperoxide isomerase (HPI) activity. These results offer important insights into the catalytic mechanism and functional versatility of Ma-LOX, underscoring its potential for a broad range of biotechnological applications.

Introduction

Lipoxygenases (LOXs) are widespread non-heme iron (or occasionally manganese) dependent enzymes that catalyze the regio- and enantioselective insertion of molecular oxygen into polyunsaturated fatty acids (PUFAs), forming fatty acid hydroperoxides (FAHPs). The specific positioning of the hydroperoxide group in the formed FAHPs gives significant prospects for further functionalization. For example, FAHP regioisomers can be converted into hemiacetals, which subsequently undergo spontaneous cleavage to produce aldehydes of varying chain lengths [1]. Derivatives of the resulting aldehydes can serve as building blocks for various biobased polymers and chemicals, whose properties will be affected by their chain length [2,3]. These aldehydes, along with alcohols derived from them, are valuable compounds in the food and flavor industries [1]. In addition to regiospecificity, the

enantioselectivity of LOXs is a key feature influencing their applications, particularly in oxylipin production. Most biologically active oxylipins exist in distinct chiral forms, and their bioactivity appears to be influenced by chirality [4–7]. Consequently, there is significant interest in the enantioselective production of oxylipins using LOXs.

In addition to producing the primary FAHP products, LOXs are also capable of producing secondary oxidation products during the activation of their non-heme iron cofactor [8]. This activation process involves redox cycling of the catalytic iron between the ferrous (Fe 2*) and ferric (Fe 3*) states, which is essential for initiating and sustaining LOX catalytic activity. Newly purified LOXs are generally isolated in the catalytically inactive ferrous form (LOX–Fe 2*) and require oxidation, typically by FAHPs generated through auto-oxidation, to convert into the active ferric state (Fig. 1) [9,10]. During this activation process, the ferrous form of the enzyme catalyzes homolytic cleavage of the O–O

E-mail address: marie.hennebelle@wur.nl (M. Hennebelle).

^{*} Corresponding author.

bond in the FAHP substrate, generating an alkoxy radical that undergoes intramolecular cyclization to form an epoxyallylic radical. Concurrently, one oxygen atom from the hydroperoxide is transferred to the enzyme, resulting in the formation of a LOX-Fe³⁺-OH complex [11]. The resulting radical species is then released through an oxygen-dependent mechanism, yielding an epoxy-allylic hydroperoxide, which can subsequently rearrange into an epoxy-allylic ketone [8]. The free ferric enzyme (LOX-Fe³⁺-OH), which is active towards PUFAs, then enters the dioxygenase catalytic cycle [12]. LOX activation is typically a single-turnover process, wherein the enzyme, once oxidized to its ferric form, remains in that state and no longer reacts with FAHPs [13]. An exception to this rule is human epidermal LOX3 (eLOX3), which exhibits hydroperoxide isomerase (HPI) activity [11]. Through this activity, the ferrous form of eLOX3 converts FAHPs into epoxy alcohols or ketones and is subsequently regenerated to its reduced ferrous state upon product release [8,11]. Although ketones are not structural isomers of FAHPs, both epoxy alcohols and ketones are considered as products of HPI activity [11].

In addition to human eLOX3, HPI activity has been reported in a limited number of other LOXs under specific conditions. For instance,

soybean LOX-1 exhibits HPI activity when exposed to high concentrations of FAHPs or under anaerobic condition [14,15]. In the manganese-containing LOX from the fungus *Gaeumannomyces avenae*, this activity is enhanced by the G316A mutation, which alters the positioning of molecular oxygen within the active site [16]. However, data on the prevalence of HPI activity among other LOXs remain scarce. The occurrence of HPI activity is of particular interest, as the resulting unsaturated epoxy alcohols can serve as key intermediates in the synthesis of bioactive compounds such as 1,3-diols, leukotrienes, and mueggelone [17–20].

The promising industrial applications of LOX have driven the exploration of this enzyme from diverse biological sources. Although most mechanistic and structural knowledge was originally obtained from studies on eukaryotic LOXs [21–29], bacterial LOXs have attracted growing interest in recent years due to their broad substrate scope toward various PUFAs [30–37]. Moreover, bacterial LOXs exhibit distinct regioselectivities, influenced by factors such as the length and number of double bonds of the substrate, as well as the position of its double bonds [32–34,36–38]. Bacterial LOXs showing either *S* [31–34] or *R* enantioselectivity [36,38,39] have been reported. Some bacterial LOXs have

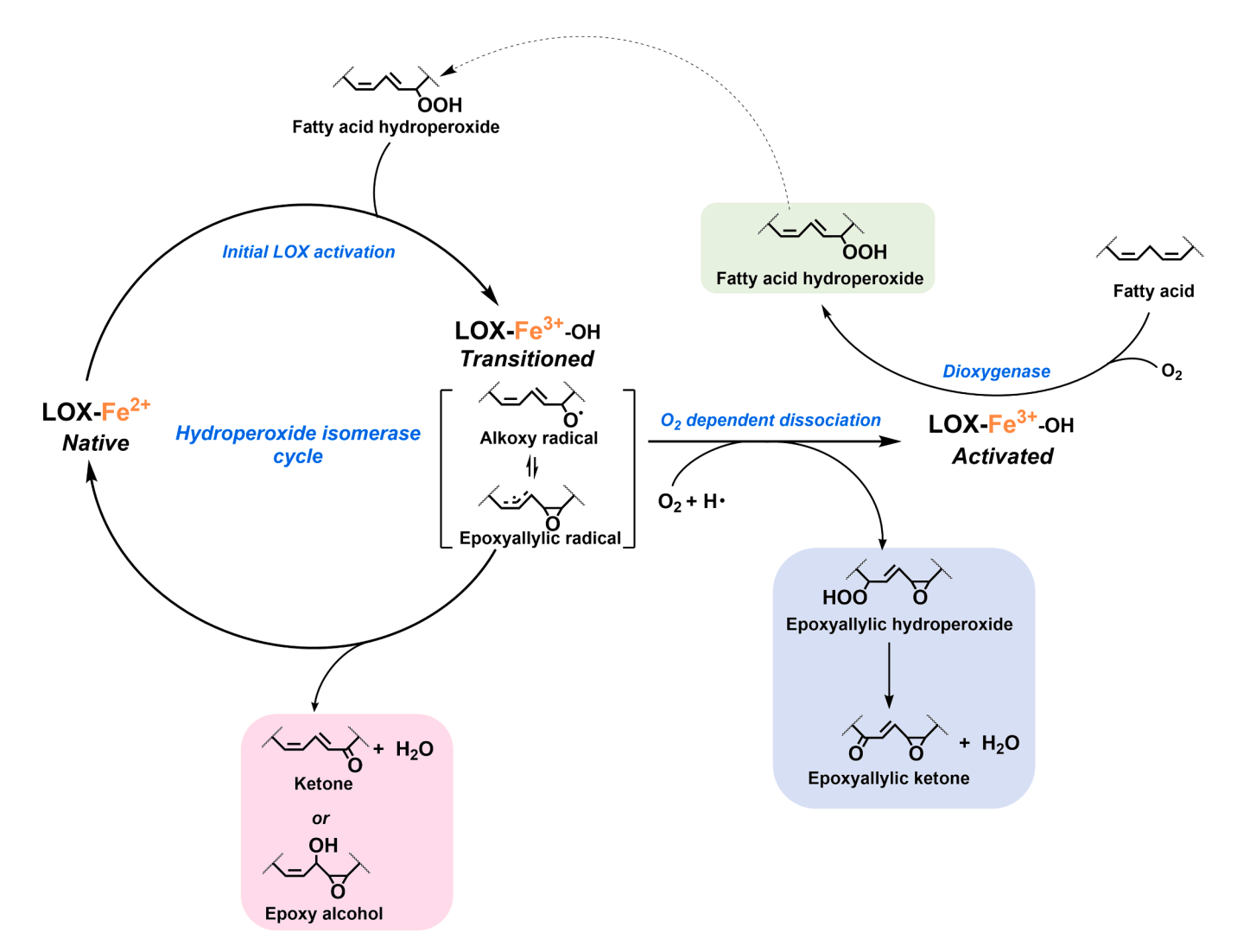


Fig. 1. Initial LOX activation and subsequent dioxygenase or hydroperoxide isomerase (HPI) activity. Activation of the LOX non-heme iron cofactor by FAHPs, typically formed via auto-oxidation, leads to the generation of an alkoxy or epoxy-allylic radical intermediate. This intermediate undergoes oxygen-dependent dissociation to yield an epoxy-allylic hydroperoxide, which is further converted into an epoxy-allylic ketone (illustrated in the blue box). Once in the ferric state, the enzyme catalyzes the dioxygenation of PUFAs to produce FAHP as the primary product (green box). In cases where LOX exhibits HPI activity, the radical intermediate can alternatively be converted into an epoxy alcohol or ketone (pink box), with concurrent regeneration of the enzyme's ferrous state upon product release. When this regeneration occurs continuously, the FAHP generated by dioxygenase activity can serve to reactivate the enzyme, as indicated by the dashed arrow. The figure is adapted from [8] with slight modifications.

also been found to catalyze double dioxygenation reactions [32,40–42], which has gained attention due to the potential inflammation-resolving activity of dihydroxy fatty acids that can be derived from the double dioxygenation products [43,44]. Despite their vast potential, a significant knowledge gap exists regarding bacterial LOXs: while over 10,500 protein sequences from bacterial kingdom have been annotated in the NCBI protein database (accessed in October 2025) as LOX or as proteins containing LOX-like domains, only a handful of bacterial LOXs have undergone thorough biochemical characterization [35]. Consequently, to harness the full potential of bacterial LOXs and broaden their application, further exploration and characterization of new bacterial LOXs is required.

Our previous analysis of bacterial LOX clustering and phylogenetic relationships revealed nine distinct groups, each defined by conserved residues that govern regioselectivity and structural features [35]. According to the clustering findings, while almost all bacterial LOX clusters only contain the helical catalytic domain, two clusters of bacterial LOXs (cluster 3 and 6) contain both the N-terminal β -barrel domain and the C-terminal helical catalytic domain, similar to eukaryotic LOXs [35]. Interestingly, while LOXs from cluster 3 exhibit a similar overall structure to eukaryotic LOXs, those from cluster 6 show slight structural differences. In cluster 6, the β -barrel domain position shifts relative to the helical catalytic domain, and there is an N-terminal helical extension, as observed in some other bacterial LOX clusters. This distinct structure is exemplified by one of the well-characterized LOXs from this cluster, *Cyanothece* sp. LOX (Fig. 2A) [36]. These unique structural characteristics, showing similarities to both eukaryotic and other

bacterial LOXs, suggest that this cluster may represent an evolutionary transition from bacterial to eukaryotic LOXs, prompting further characterization of LOXs from this cluster.

The LOX domain-containing protein from *M. aeruginosa* (WP_046663104.1), from here on referred to as Ma-LOX, is classified as one of the putative bacterial LOXs within cluster 6 [35]. Ma-LOX exhibits 37.8 % sequence identity to the well-characterized *Cyanothece* sp. LOX (WP_012595715.1) [36]. Despite this relatively low sequence identity, Ma-LOX has been predicted to have an overall structure similar to that of *Cyanothece* sp. LOX [35] (Fig. 2A). However, the N-terminal helical extension of the predicted structure (shown in light pink), which has a low confidence score (Fig. S1), has a different orientation than that of *Cyanothece* sp. LOX.

LOX regioselectivity is governed by distinct structural features of the enzyme, including the architecture of the oxygen migration channel, which guides molecular oxygen to the active site [23,45–47], and the depth of the substrate-binding pocket [48]. A confined oxygen migration channel directs the oxygen molecule to a specific position, while a more spacious channel allows dioxygenation to occur at multiple positions [24,45]. The depth of the substrate-binding pocket is modulated by the size of amino acid residues positioned at its base [49–51]. When bulky amino acids are present, the substrate binds more superficially compared to when smaller residues are present. In the crystal structure of *Cyanothece* sp. LOX (PDB 5EK8), the residues at the bottom of the binding pocket were identified (Fig. S2). Sequence alignment between *Cyanothece* sp. LOX and Ma-LOX suggests that three of the bottom residues differ in size between the two enzymes (Fig. 2B). These differences

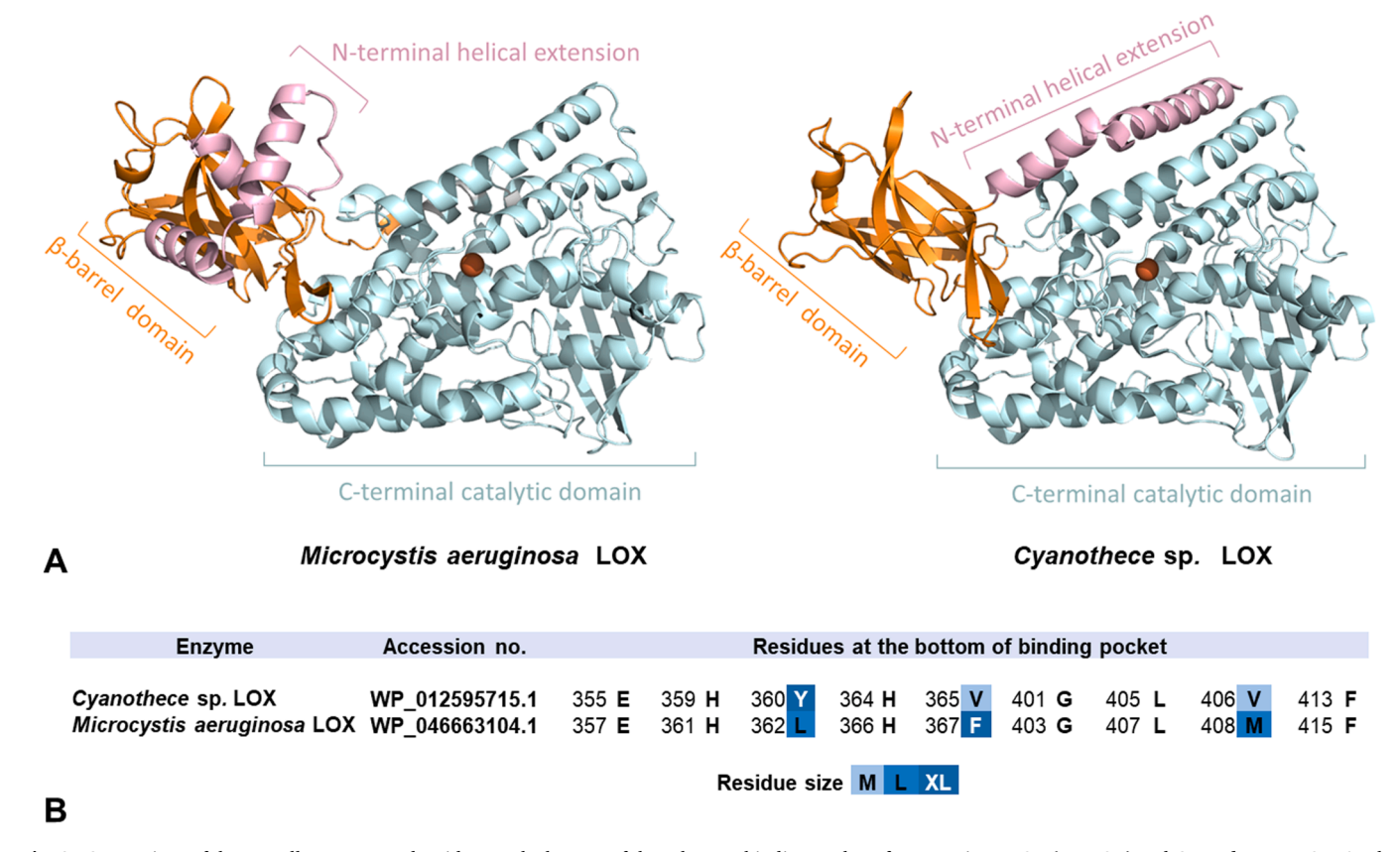


Fig. 2. Comparison of the overall structure and residues at the bottom of the substrate-binding pocket of M. aeruginosa LOX (Ma-LOX) and Cyanothece sp. LOX. A. The predicted three-dimensional structure of M. aeruginosa LOX (Ma-LOX), which was modeled using Alphafold2 [35] (left) and the crystal structure of Cyanothece sp. LOX (PDB: 5EK8) (right). The position of the non-heme iron (depicted as an orange sphere) in the Ma-LOX active site was determined by superimposing the AlphaFold-predicted structure of Ma-LOX with the crystal structure of Cyanothece sp. LOX, which shares 37.8 % sequence identity. Light pink highlights the N-terminal helical extension, orange indicates the N-terminal β-barrel domain, and light cyan represents the C-terminal catalytic domain. B. Sequence alignment of Ma-LOX and Cyanothece sp. LOX, showing the residues that are present at the bottom of the substrate binding pocket with their corresponding sequence number. Residues are color-coded according to their size: medium (M, 101–140 ų), large (L, 141–180 ų), and extra-large (XL, 181–230 ų), with shades ranging from light to dark blue.

could potentially influence substrate specificity and regioselectivity.

This study focused on elucidating the biochemical characteristics of Ma-LOX, including its substrate scope as well as the regio- and enantioselectivity of its dioxygenation activity. In addition, we investigated the occurrence of secondary products in Ma-LOX catalyzed reactions. The insights obtained have deepened our knowledge of the catalytic mechanisms and capabilities of bacterial LOXs, thereby broadening the perspectives for their potential application as sustainable eco-friendly alternatives in the food, pharmaceutical, and biobased chemical industries.

Materials and methods

Materials

The lipoxygenase gene from *M. aeruginosa* (Ma-LOX) (NCBI WP_046663104.1), with codons optimized for heterologous expression in *Escherichia coli* (Table S1), was synthesized by GenScript Biotech (Rijswijk, The Netherlands). This gene was inserted into the pET-19b expression plasmid (Novagen, USA) using the *NdeI* and *BlpI* restriction sites, incorporating an N-terminal deca-histidine (10x His) tag to enable affinity purification (Fig. S3).

For recombinant expression, the construct was transformed into $\it E.~coli~BL21(DE3)$ cells (Invitrogen, California, USA). The bacterial cultures were cultivated in Luria Bertani (LB) medium containing ampicillin sodium salt (Sigma-Aldrich, Missouri, USA), and gene expression was induced with isopropyl β -D-1-thiogalactopyranoside (IPTG, Duchefa Biochemie B.V., Haarlem, The Netherlands). Cell disruption was performed using BugBuster reagent (Millipore-Merck, Darmstadt, Germany), with protease activity suppressed by the addition of cOmplete EDTA-free inhibitor tablets (Roche, Mannheim, Germany) and Pepstatin A (Sigma-Aldrich). The His-tagged enzyme was purified via Ni-NTA affinity chromatography (Millipore-Merck), and concentrated using VivaSpin concentrators (GE Healthcare, Buckinghamshire, UK).

Reagents for enzymatic assays and product characterization were sourced from various suppliers. PUFAs including linoleic acid (LA; C18:2 $\Delta 9Z,12Z$), α -linolenic acid (ALA; C18:3 $\Delta 9Z,12Z,15Z$), γ -linolenic acid (GLA; C18:3 $\Delta 6Z,9Z,12Z),$ arachidonic acid (AA, C20:4 C20:5 $\Delta 5Z, 8Z, 11Z, 14Z),$ eicosapentaenoic acid (EPA, (DHA. C22:6 $\Delta 5Z, 8Z, 11Z, 14Z, 17Z),$ docosahexaenoic acid $\Delta 4Z$,7Z,10Z,13Z,16Z,19Z) were obtained from Nu-Chek Prep, Inc., Minnesota, USA. Standards for fatty acid hydroperoxide including 13 (S)-hydroperoxy-9Z,11E-octadecadienoic acid (13-HPODE), 13(S)hydroperoxy-9Z,11E,15Z-octadecatrienoic acid (13-HPOTrE), 15(S)hydroperoxy-5Z,8Z,11Z,13E-eicosatetraenoic acid (15-HPETE), 12(S)hydroperoxy-5Z,8Z,10E,14Z,17Z-eicosapentaenoic acid (12-HPEPE), and 17(S)-hydroperoxy-4Z,7Z,10Z,13Z,15E,19Z-docosahexaenoic acid (17-HPDHE), were supplied by Larodan, Solna, Sweden. In addition, analytical standards of possible enzymatic products, including 13(S)and 13(R)-hydroxy-9Z,11E-octadecadienoic acid (13S- and 13R-HODE), 13-oxo-9Z,11E-octadecadienoic acid (13-oxoODE), cis-12(13)-epoxy-9Z-octadecenoic acid (12(13)-EpOME), 13-oxo-9Z,11E,15Z-octadecatrienoic acid (13-oxoOTrE), and cis-12(13)-epoxy-9Z,15Z-octadecadienoic acid (12(13)-EpODE) were also acquired from Larodan, Solna, Sweden. Additional chemicals such as xylenol orange tetrasodium salt, iron(II) sulfate heptahydrate, perchloric acid, cumene hydroperoxide, and cysteine were purchased from Sigma-Aldrich (Missouri, USA). Solvents used for ULC/MS analysis, including acetonitrile, methanol (absolute), ethyl acetate, and glacial acetic acid, were procured from Biosolve B.V. (Valkenswaard, The Netherlands).

Gene expression and enzyme purification

E. coli BL21(DE3) cells transformed with the pET-19b_Ma-LOX construct were cultured in Luria Bertani (LB) medium at 37 $^{\circ}$ C under constant agitation at 250 rpm. As a negative control, cells carrying the

empty pET-19b plasmid were grown under identical conditions. Once the culture reached an optical density at 600 nm (OD $_{600}$) of approximately 0.6–0.8, gene expression was induced by the addition of 0.5 mM IPTG. The cultures were then maintained at 16 °C with reduced shaking speed (150 rpm) for an additional 48 h. After induction, the cells were collected by centrifugation at 7000 \times g for 15 min at 4 °C and stored at –20 °C until further purification steps.

The purification of Ma-LOX began by thawing and resuspending frozen E. coli cell pellets derived from a 200 mL culture volume in a lysis buffer. This buffer was composed of 10 mL BugBuster Master Mix supplemented with one tablet of cOmplete EDTA-free protease inhibitor cocktail and 1 μ M pepstatin A. The lysate was clarified by centrifugation at $16,000 \times g$ for 20 min at 4 °C, and the resulting supernatant was passed through a $0.22\,\mu m$ filter to eliminate remaining particulates. The clarified lysate was subjected to affinity purification using a gravity-flow column packed with 1 mL of Ni-NTA His-bind resin. Before loading the protein extract, the resin was pre-equilibrated with 10 column volumes (CV) of buffer containing 50 mM sodium phosphate (NaH₂PO₄), 300 mM sodium chloride (NaCl), and 10 mM imidazole at pH 7.0. The filtered supernatant was then applied to the column. Once fully absorbed, sequential washes were performed using 2 CV each of wash buffers (pH 7.0), all containing 50 mM NaH₂PO₄ and 300 mM NaCl but with increasing imidazole concentrations: 20, 50, 100, and 150 mM. Protein was subsequently eluted using 4 CV of elution buffer containing 250 mM imidazole under identical buffer conditions. Elution fractions were desalted and concentrated using a VivaSpin centrifugal concentrator (10 kDa molecular weight cutoff). The purified Ma-LOX enzyme was stored in 100 mM Bis-Tris buffer pH 7.0 in an ice bath, and kept at 4 °C before use. Protein concentrations were quantified via the Bradford assay [52].

Molecular mass and iron content determination

The apparent molecular mass of the purified enzyme subunit was assessed by SDS-PAGE using a NuPAGE 10 % Mini Protein Gel (Invitrogen, USA), with SeeBlue Plus2 pre-stained standard (Invitrogen, USA) as molecular weight standards. The native molecular mass of the enzyme was estimated by gel filtration chromatography on a Superdex 200 Increase 10/300 GL column (Cytiva, the Netherlands). A 75 μL aliquot of the enzyme solution (2.85 mg/mL) was injected into the column and eluted with a 20 mM phosphate buffer (pH 7.0) containing 150 mM NaCl at a flow rate of 0.75 mL/min. Calibration of the column was conducted with thyroglobulin (669 kDa), ferritin (440 kDa), aldolase (158 kDa), and conalbumin (75 kDa). The elution volume of blue dextran (2000 kDa) was used to determine the void volume. Comparison of the retention time of the purified Ma-LOX with that of the reference proteins allowed determination of its relative molecular mass. The partition coefficient (K_{AV}) was calculated using Eq. 1 [53], where V_0 is the void volume, V_t is the total volume of the column, and V_e is the elution volume.

$$KAV = \frac{Ve - Vo}{Vt - Vo} \tag{1}$$

The purified Ma-LOX, with a concentration of 205 egg/mL (2.71 $\mu M)$ dissolved in 100 mM Bis-Tris buffer at pH 7.0, was used to determine the iron content in the enzyme. For the control, the purified fraction from E. coli BL21(DE3) containing an empty plasmid, which underwent the same overexpression and purification procedures as Ma-LOX, was used. The iron content of the purified Ma-LOX and the control was measured in duplicate using ICP-MS (SGS Nederland B.V., Spijkenisse, the Netherlands). The iron load (%) was determined by dividing the quantified iron content (μ mol/L) by the enzyme concentration (μ mol/L) and multiplying the result by 100.

Preparation of PUFA substrates

PUFAs were solubilized and freshly prepared using a previously reported protocol, with slight modifications [54]. In a 10 mL volumetric flask, each PUFA substrate (LA, ALA, GLA, AA, EPA, or DHA) was dissolved in 4 mL of Milli-Q water containing 12.5 μL of Tween-20. To aid solubilization, 0.55 mL of 0.5 M sodium hydroxide (NaOH) was added, leading to a clear solution. The volume was then brought up to 10 mL with Milli-Q water, yielding a final PUFA concentration of 4.33 mM.

LOX activity measurement using FOX assay

Enzyme activity was assessed through the ferrous-oxidized xylenol orange (FOX) assay, as previously described [55]. A freshly prepared FOX reagent was used, consisting of 2.0 mM ferrous sulfate, 0.29 mM xylenol orange tetrasodium salt, and 440 mM perchloric acid, dissolved in a methanol-to-water ratio of 9:1. The reaction mixtures consisted of 30 μL of PUFA substrate and 5 μL of enzyme solution dissolved in 100 mM Bis-Tris buffer pH 7.0 to a final volume of 500 μ L, resulting in final concentrations of 260 µM substrate and 23 nM enzyme. For the negative control (blank), the enzyme solution was substituted with the same volume of buffer. Following a 5-minute incubation at room temperature, 30 µL of both sample and blank were transferred into wells of a 96-well plate and mixed with 150 µL of the FOX reagent. The mixtures were incubated at room temperature for an additional 15 min to allow color development. Absorbance was subsequently recorded at 570 nm using a Spectramax ID3 plate reader (Molecular Devices, LLC, California, USA). Hydroperoxide concentrations were quantified using a calibration curve constructed with cumene hydroperoxide (CuHP). Due to differences in reactivity among fatty acid hydroperoxides (FAHPs) in the FOX assay, correction factors were applied to achieve accurate quantification. These factors were calculated by dividing CuHP's molar extinction coefficient by that of each respective FAHP. The correction values used were: 1.24 for HPODE, 1.29 for HPOTE, 1.40 for HPETE, 1.96 for HPEPE, and 1.80 for HPDHE [55]. Enzyme activity was expressed in units (U), where one unit corresponds to the formation of 1 µmol of hydroperoxide per minute. Specific activity (U/mg) was calculated by dividing the activity by the amount of enzyme used in milligrams. Specific activity based solely on the catalytically active (iron-loaded) form of the enzyme was determined by accounting for its iron content.

Determination of optimum conditions and substrate preference of the enzyme

The optimal pH and temperature conditions for Ma-LOX activity were evaluated using LA as the substrate. For pH profiling, reactions were carried out at room temperature (\sim 20 °C) in a series of buffers: 100 mM citrate buffer (citric acid/sodium citrate) for pH 3.0, 4.0, and 5.0; 100 mM Bis-Tris buffer (Bis-Tris/HCl) for pH 6.0 and 7.0; and 100 mM Tris-HCl buffer (Tris base/HCl) for pH 8.0, 9.0, and 10.0. Temperature dependence was assessed by incubating the enzymatic reactions at 20, 30, 40, and 50 °C in the pH-optimal buffer (100 mM Bis-Tris pH 7.0).

To determine the substrate preference of Ma-LOX, enzymatic reactions were performed at 30 °C in 100 mM Bis-Tris buffer at pH 7.0 using different PUFAs (LA, ALA, GLA, AA, EPA, or DHA). To maintain the absorbance within the linear range of the calibration curve, the volume of the enzyme solution added during the enzymatic assay was adjusted according to the substrate used due to significant differences in the enzyme activity toward different substrates. When using LA or ALA as substrate, 5 μL of the enzyme solution was used, giving a final concentration of 23 nM of enzyme. However, when using GLA, AA, EPA or DHA as substrate, 25 μL of enzyme solution was used, giving a final concentration of 115 nM of enzyme.

Hydroperoxides concentration produced in the above reactions was

determined using the FOX assay. All assays were conducted in six biological replicates. The results were statistically analyzed using the nonparametric Kruskal–Wallis test using SPSS Statistics 28.0 (IBM Corp.).

Sample preparation for dioxygenation regioselectivity analysis

Enzymatic reactions for determining the regioselectivity of dioxygenation leading to primary product formation were conducted in a total volume of 1.0 mL, consisting of 40 μ L Ma-LOX (150 μ g/mL), 240 μ L PUFA (4.33 mM; including LA, ALA, GLA, AA, EPA, or DHA), and 720 μL of 100 mM Bis-Tris buffer at pH 7.0. This yielded final concentrations of 6 μg/mL enzyme and 1.04 mM substrate. Negative control reactions, lacking enzyme, were prepared by mixing the same amount of PUFA with 760 μL of 100 mM Bis-Tris buffer pH 7.0. Reactions were incubated at 30 $^{\circ}$ C for 20 h with shaking at 300 rpm. To terminate the reaction and extract lipid products, the reaction mixture was transferred into a Kimax tube containing 5 mL of ethyl acetate and vortexed briefly [34]. The mixture was centrifuged at $5000 \times g$ for 15 min at room temperature, resulting in three distinct layers: an aqueous phase at the bottom, denatured protein at the interface, and an organic phase on top. Following centrifugation, 4 mL of the upper layer was collected and evaporated under a nitrogen flow at 30 °C. Once the ethyl acetate had completely evaporated, the dried extract was then resuspended in 2 mL of methanol and stored at -80 °C until analysis using reversed-phase ultra-high-pressure liquid chromatography photodiode array high-resolution mass spectrometry (RP-UHPLC-PDA-HRMS).

Sample preparation for secondary products analysis

To investigate the formation of secondary products during the enzymatic reaction of Ma-LOX, LA and ALA were utilized as substrates. This study evaluated the influence of enzyme concentration and incubation time on the generation of secondary metabolites. To assess the effect of enzyme concentration, 20, 40, or 60 µL of Ma-LOX solution (150 μg/mL) was combined with 100 μL of 4.33 mM PUFA and diluted to a final volume of 1.0 mL using 100 mM Bis-Tris buffer (pH 7.0), yielding final enzyme concentrations of 3, 6, or 9 μg/mL, respectively, and a substrate concentration of 433 μM . Negative control reactions (enzyme-free) were prepared using an identical amount of substrate and adjusted to 1.0 mL with buffer. The reaction mixtures were incubated at 30 °C for 1 h with shaking at 300 rpm. Lipid extraction was performed using the same protocol as described above. To examine the effect of incubation time, 40 μ L of Ma-LOX (150 μ g/mL) and 100 μ L of 4.33 mM PUFA were diluted with 100 mM Bis-Tris buffer (pH 7.0) to a final volume of 1.0 mL, resulting in a final enzyme concentration of 6 µg/mL and a substrate concentration of 433 μ M. Reactions were incubated at 30 °C for 1, 2, 3, and 18 h, respectively. Negative controls for each time point were prepared by replacing the enzyme with buffer and processed under identical conditions. After incubation, the lipid fractions were extracted using the same protocol as described above prior to RP-UHPLC-PDA-HRMS analysis.

Product characterization using RP-UHPLC-PDA-HRMS

The products formed from enzymatic reactions were characterized using an ultra-high-performance liquid chromatography system (UHPLC; Thermo Vanquish, Thermo Fisher Scientific, Pittsburgh, PA, USA) paired with a photodiode array (PDA) detector and a Q Exactive Focus Hybrid Quadrupole-Orbitrap Fourier Transform mass spectrometer (FTMS) (Thermo Fisher Scientific). Separation was carried out on a reversed-phase Acquity UPLC BEH C18 column (2.1 \times 150 mm, 1.7 μm particle size; Waters Corporation, Milford, MA, USA). The column compartment was maintained at 25 $^{\circ}$ C, and samples were injected using an autosampler held at 10 $^{\circ}$ C. A constant flow rate of 350 $\mu L/min$ was applied throughout the analysis. Chromatographic separation utilized

two mobile phases: solvent A (ultrapure water with 0.01 % v/v acetic acid) and solvent B (acetonitrile containing 0.01 % v/v acetic acid). The gradient elution was programmed as follows: 50 % B for the initial 1.25 min, then linearly ramped to 90 % B up to 51.43 min, followed by an increase to 100 % B between 51.43 and 52.68 min. The composition was held at 100 % B until 58.90 min, then decreased to 50 % B by 60.21 min and maintained at this composition until 66.48 min to reequilibrate the system. Mass spectrometric detection was performed in negative ion mode using a Heated Electrospray Ionization (HESI) source. Instrument parameters included a capillary temperature of 250 °C, an ion spray voltage of 2.5 kV, and a sheath gas pressure set to 45 psi. Fullscan mass spectra were acquired in discovery mode across an m/z range of 250-1000 with a resolution power of 70,000. Fragmentation was performed via Higher-energy Collisional Dissociation (HCD), with normalized collision energies of 35 % for detecting products derived from AA, EPA, and DHA, and 45 % for those from LA, ALA, and GLA. All acquired data were processed and analyzed using Xcalibur software version 4.5 (Thermo Fisher Scientific).

Identification of the primary products was based on the detection of peaks with molecular masses corresponding to the expected FAHPs derived from each PUFA. To confirm the identity of these FAHP peaks, UV absorbance at 234 nm was examined, indicative of the presence of a conjugated diene moiety [56]. The positional specificity of the hydroperoxide group on the fatty acid was elucidated based on diagnostic HCD fragments which arose from cleavage of carbon–carbon bonds adjacent to the hydroperoxide group and/or allylic to the double bond [57,58]. Enzyme regioselectivity was determined by evaluating the distribution of FAHP isomers based on their relative peak areas. Data from control reactions without enzyme were used to account for contributions from non-enzymatic auto-oxidation. The proportion of each FAHP isomer was calculated using Eq. 2:

$$Relative \ abundance(\%) = \frac{(A_s - A_c)}{(TA_s - TA_c)} \times 100$$
 (2)

where A represents the peak area of an individual FAHP isomer, TA is the total peak area of all detected FAHPs, and subscripts s and c denote sample and negative control, respectively.

Identification of the secondary products was done by analyzing the remaining peaks with specific masses corresponding to possible secondary products derived from LA and ALA. These specific mass peaks were then evaluated for their fragmentation pattern. Confirmation of epoxy alcohols was carried out by assessing specific fragments resulting from the cleavage of the C-C bond located near the epoxide and hydroxide group [8]. Confirmation of ketones was carried out by comparing them with the retention time and fragmentation pattern of the corresponding standard compounds (13-oxoODE and 13-oxoOTrE, respectively). Identification of other ketone regioisomers (i.e., 9-oxoODE and 9-oxoOTrE) was done by assessing the fragments resulting from the same cleavage pattern as their regioisomers. Other secondary products than epoxy alcohols and ketones were identified based on their masses and fragmentation pattern. Additionally, further confirmation of secondary products with a ketone and/or a conjugated diene moiety was achieved by assessing their absorbance at 282 nm [16] and 234 nm [56], respectively.

Analysis of dioxygenation enantioselectivity

The dioxygenation enantioselectivity of Ma-LOX was determined using LA as substrate in three biological replicates. The enzymatic reactions and sample extractions were performed as described for regioselectivity analysis. The LA hydroperoxide in the extracted enzymatic product was then reduced to its hydroxy form by dissolving it in a 10 mM cysteine solution prepared in 100 mM phosphate buffer (pH 8.0). The mixtures were incubated for 10 min on a rotary shaker at room temperature. They were then acidified with glacial acetic acid until the

pH reached 3.0. The acidified solutions were transferred to Kimax tubes containing 3 mL of ethyl acetate and vortexed. The mixtures were then centrifuged at 5000 \times g for 15 min at room temperature. After centrifugation, 2.5 mL of the upper organic phase was carefully collected and evaporated under a nitrogen flow at 30 °C. Once the ethyl acetate was fully removed, the residues were reconstituted in 1 mL of methanol and stored at –80 °C for subsequent analysis. Samples were analyzed using a Waters Alliance 2695 HPLC. Eluting compounds were detected with a UV–vis detector at 234 nm. 13-HODE enantiomers were separated using a Phenomenex Lux cellulose-1 column (4.7 mm×250 mm, 5 μ m particles) operated at 30°C. As eluent, a mixture of 97 % v/v hexane, 3 % v/v isopropanol and 0.025 % v/v glacial acetic acid was used at a flow rate of 0.5 mL/min. Enantiomeric excess (ee) was calculated based on peak areas using Eq. 3:

$$ee = R - S \tag{3}$$

where R and S represent the relative abundances of the R- and S-enantiomers, respectively. All values are expressed as percentages.

Structure modelling and docking of substrates

The three-dimensional structure of Ma-LOX was predicted using AlphaFold2 [59] with the casp14 settings. In order to visualize the substrates binding in the enzyme's binding pocket and confirm the experimental results of regioselectivity, molecular docking was conducted using Molecular Operating Environment (MOE) version 2022.02 (Chemical Computing Group, Montreal, QC, Canada). The structures of PUFAs and HPOTrEs were retrieved from the PubChem database. Prior to docking, the ligand structures were subjected to energy minimization and appropriate protonation state adjustments. These steps were performed using the Amber10:EHT force field with MOE's default settings. To prepare the Ma-LOX model for docking, an iron atom was incorporated into the predicted structure, and its valency was appropriately assigned. The Ma-LOX-Fe complex was then refined by energy minimization under experimental-like conditions: pH 7.0, ionic strength of 100 mM, and a temperature of 25 $^{\circ}$ C. Residues predicted to coordinate with the iron atom were selected based on the iron-binding configuration reported in the lipoxygenase from Cyanothece sp. (PDB ID: 5EK8). The prepared substrates were subsequently docked into the Ma-LOX active site region encompassing the iron-coordinating residues (H361, H366, H571, H575, and S668), which define the catalytic pocket around the metal center. Docking was performed using triangle matcher placement and induced fit refinement settings. Binding affinity was evaluated using the London dG scoring function, where more negative S-scores reflected stronger predicted interactions. Docking simulations were performed in duplicate, with each run generating 30 possible poses. The five poses with the lowest binding scores were selected for further analysis. Final pose selection was based on multiple criteria: minimal S-score, Root Mean Square Deviation (RMSD) of ≤ 2 Å, and favorable proximity between the hydrogen abstraction site and the iron center.

Results

Biochemical properties of Ma-LOX

Ma-LOX was purified from recombinant *E. coli* cells expressing the *lox* gene using Ni-NTA affinity chromatography. The enzyme was recovered in a soluble form and displayed a single band on SDS-PAGE, corresponding to an apparent subunit molecular mass of approximately 75 kDa, as estimated from its electrophoretic migration profile (Fig. S4A). This observed mass closely aligns with the theoretical mass of Ma-LOX (668 amino acids), which is predicted to be 79.5 kDa when accounting for the added enterokinase site and 10 histidine residues. Analysis of the protein by gel filtration chromatography (Fig. S4B)

indicated that Ma-LOX mainly exists as a dimer in solution. However, the presence of monomeric, oligomeric and higher polymeric forms of the protein was also observed (Fig. S4C). Based on ICP-MS analysis, the purified Ma-LOX had an iron load of 76 % (Table S2). pH and temperature optima for Ma-LOX activity were determined using LA as a substrate. The tested pH ranged from 3.0 to 9.0 at room temperature (~20 °C), and the temperature ranged from 20 to 50 °C (pH 7.0). Ma-LOX displayed its highest activity between pH 5.0 and 7.0 and at 30 °C (Fig. S5A,B).

Substrate preference, dioxygenation regioselectivity and enantioselectivity of Ma-LOX

The evaluation of Ma-LOX substrate preference was conducted at 30 °C using PUFA substrates with varying carbon chain lengths (C18 to C22), numbers of double bonds (2–6), and position of the first double bond (ω -3 or ω -6). Six different PUFAs were employed: LA (C18:2, ω -6), ALA (C18:3, ω -3), GLA (C18:3, ω -6), AA (C20:4, ω -6), EPA (C20:5, ω -3), and DHA (C22:6, ω -3). Ma-LOX displayed the highest specific activities for LA and ALA, followed by DHA, and the lowest specific activities for GLA, AA, and EPA (Fig. 3A).

To determine the positions of the hydroperoxide groups in FAHPs generated by Ma-LOX from the six PUFAs, RP-UHPLC-PDA-HRMS was employed. The FAHP regioisomers were identified based on their specific masses and fragmentation patterns in MS^2 spectra. Chromatographic peaks of FAHPs were identified based on m/z values, as well as their absorbance at 234 nm, corresponding to the presence of

conjugated diene moieties. The retention times, masses, relative abundances, and diagnostic $\rm MS^2$ fragments of FAHPs generated by Ma-LOX are summarized in Table S3. Representative chromatograms and fragmentation spectra are shown in Fig. S6 and S7, respectively. Ma-LOX exhibited distinct dioxygenation regioselectivity toward different PUFA substrates, producing products predominantly oxygenated at the ω -5 position in LA, ALA, GLA, and AA (Fig. 3B), with relative abundances of 96.9 %, 98.3 %, 69.3 %, and 69.3 %, respectively (Table S3). In contrast, the enzyme favored dioxygenation at the ω -2 and ω -8 positions for longer-chain substrates such as EPA and DHA (Fig. 3B). These results confirm that Ma-LOX catalyzes oxygen insertion with substrate-dependent positional specificity.

Chiral product analysis (Fig. 3C) showed that Ma-LOX had a strong preference for producing the *R*-enantiomer of HPODE from the LA substrate with an ee of 79 % (Table S4). Regiospecificity for ω -5 dioxygenation was also observed for GLA and AA, although to a smaller extent. The lowest regioselectivity was observed on EPA, with the most preferred dioxygenation observed at the ω -2 position. When DHA was used as a substrate, the enzyme displayed a strong preference for dioxygenation at the ω -8 position, and a lower degree of activity towards the ω -2 position.

Secondary products profile of Ma-LOX

To investigate the formation of secondary products during the enzymatic reaction of Ma-LOX, the two most preferred substrates were used, i.e., LA and ALA. The RP-UHPLC-MS chromatograms from those

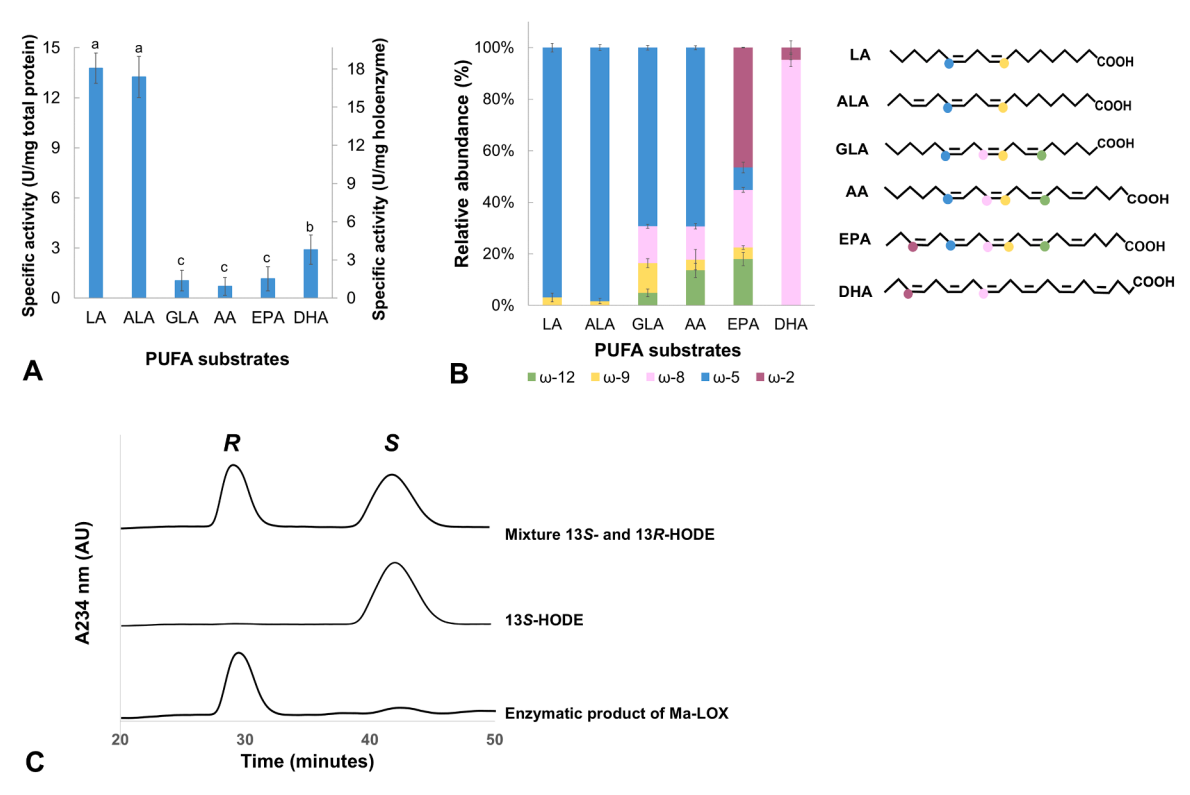


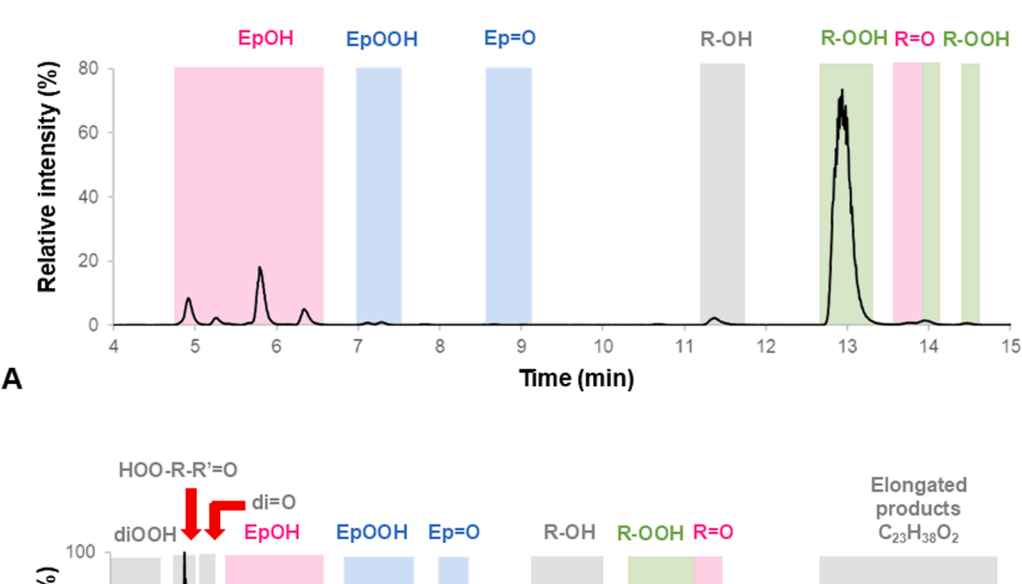
Fig. 3. Substrate preference (A), regioselectivity (B) and enantioselectivity (C) of Ma-LOX. A. Ma-LOX exhibited its highest preference for LA and ALA. Substrate preference data are presented as mean \pm standard deviation (n = 6), with different letters denoting statistically significant differences at p < 0.01. B. Relative distribution of dioxygenation positions for six different PUFAs after a 20 h incubation with Ma-LOX (left). Enzymatic reactions were performed at room temperature (~20 °C) using a final concentration of 6 μg/mL enzyme and 1.04 mM PUFA substrates dissolved in 100 mM Bis-Tris buffer (pH 7.0). Data are reported as mean \pm SD of three biological replicates. Different colors indicate different positions of the hydroperoxide group counted from the methyl end. The PUFA structures are illustrated with oxidation sites annotated based on their corresponding omega positions (right). The PUFAs used were linoleic acid (LA; C18:2 Δ9Z,12Z), α-linolenic acid (ALA; C18:3 Δ9Z,12Z,15Z), γ-linolenic acid (GLA; C18:3 Δ6Z,9Z,12Z), arachidonic acid (AA; C20:4 Δ5Z,8Z,11Z,14Z), eicosapentaenoic acid (EPA; C20:5 Δ5Z,8Z,11Z,14Z,17Z), and docosahexaenoic acid (DHA; C22:6 Δ4Z,7Z,10Z,13Z,16Z,19Z). C. Chromatogram of the reduced chiral products of Ma-LOX using LA as the substrate, compared to 13S-HODE and a mixture of 13S- and 13R-HODE standards. The chromatogram shown is representative of identical results obtained from three biological replicates.

enzymatic reactions are shown in Fig. 4. Identification and characterization of the different peaks revealed that secondary products derived from both O_2 -dependent dissociation and HPI activity were formed (Table 1). Furthermore, double dioxygenated products and their derivatives, some reduced compounds, and elongated products were also formed (Table 1). The retention time of each product, the UV absorbance wavelength, the parent ion(s) and the diagnostic fragments in MS^2 spectra used for identification are listed in Table S5.

When utilizing both LA and ALA as a substrate, small amounts of epoxyallylic hydroperoxides and epoxyallylic ketones, were detected as O2-dependent dissociation derived secondary products (Fig. 4, highlighted in blue). Several peaks corresponding to epoxy alcohols and ketones were observed for both substrates (Fig. 4, highlighted in pink), suggesting that Ma-LOX exhibits HPI activity. Several peaks that were annotated as epoxy alcohols showed identical diagnostic fragments in the MS/MS profile (Fig. S8), suggesting that multiple stereoisomers were formed [60,61]. At least four stereoisomers of the epoxy alcohol were detected, corresponding to the number that can be resolved under non-chiral UHPLC conditions. Because the column employed lacks chiral selectivity, enantiomeric pairs co-eluted and could not be individually distinguished. Comprehensive stereoisomeric resolution would require the use of chiral stationary phases or orthogonal analytical techniques such as supercritical fluid chromatography. In addition to the abovementioned products, some other secondary products were observed (Fig. 4, highlighted in grey). The reduced forms of hydroperoxides, hydroxy fatty acids (hydroxides), were detected for both substrates. When using ALA as substrate, double dioxygenation products were observed at RT 2.26 and 2.45, which were annotated as isomers of 9,

16-diHPOTrE (Table S5). Further oxidized derivatives of these products, i.e., 16-oxo-9-HPOTrE or 9-oxo-16-HPOTrE, and 9,16-dioxo-OTrE, were observed at RT 3.03 and 3.27, respectively (Table S5). The presence of a ketone group in these compounds was further confirmed by absorbance of UV light at 282 nm (Fig. S9). In addition to the double dioxygenation products, Ma-LOX also produced elongated products when using ALA as a substrate, with an m/z of 345 observed at RT 39.60–41.78 (Fig. 4B), suggesting the presence of compounds with the chemical formula of $C_{23}H_{38}O_2$ (Table S5).

To investigate further the formation of these secondary products, we examined the effect of three different enzyme concentrations (3, 6, and $9\,\mu g/mL)$ over various incubation periods (1, 2, 3, and 18 h) at 30 $^{\circ}C$ with 300 rpm agitation. Negative control reactions, containing only substrate and buffer without the addition of enzyme, were also included. The results in Fig. S10 indicate that the substrates have been fully converted into products, and increasing the enzyme concentration decreased the presence of FAHPs while slightly increasing the formation of epoxy alcohols. However, increasing the incubation time did not significantly increase the formation of epoxy alcohols, although the concentration of FAHPs still decreased over time (Fig. S11). When using ALA as the substrate, higher enzyme concentrations did not result in a significant increase in double dioxygenation products but instead led to a decrease in the primary FAHP (13-HPOTrE) and a slight increase in elongated products (Fig. S10B). Additionally, longer incubation times decreased the primary FAHP (13-HPOTrE), the double dioxygenation products, and the elongated products (Fig. S11B).



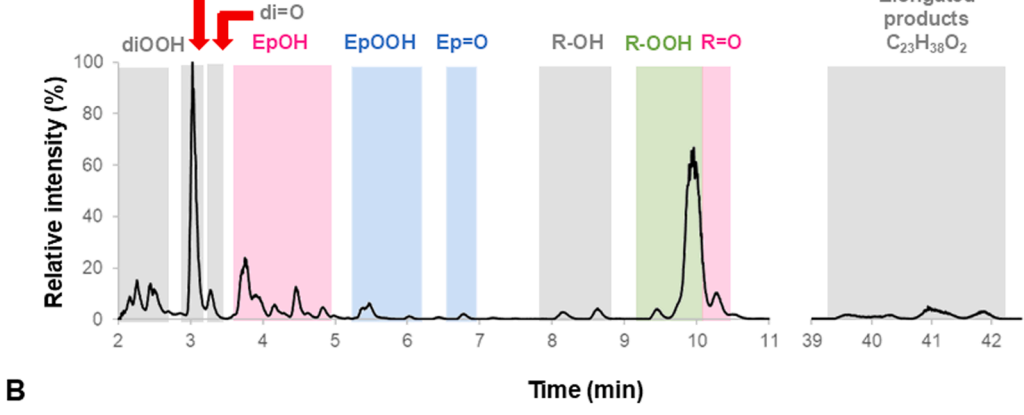


Fig. 4. RP-UHPLC-MS chromatograms of product mixtures from Ma-LOX catalyzed reactions when using LA (A) and ALA (B) as substrates incubated for 1 h at 30 °C. Identification of each peak is indicated in the figure. The primary FAHP product peaks (R-OOH) are highlighted in green; the hydroperoxide isomerase-derived product peaks: i.e., epoxy alcohols (EpOH) and ketones (R=O) are shown in pink; the O_2 - dependent dissociation derived product peaks, i.e., epoxyallylic hydroperoxides (EpOOH) and epoxyallylic ketones (Ep=O) are indicated in blue, and the other secondary product peaks: i.e., hydroxides (R-OH), di-hydroperoxides (diOOH), hydroperoxy-ketones (HOO-R-R'=O), di-ketones (di=O) and unspecific elongated products are displayed in grey.

Table 1 Secondary products observed in Ma-LOX catalyzed reactions with linoleic acid (LA) or α -linolenic acid (ALA) as substrate.

Type of products	Substrate	Product name (abbreviation)	Retention time (min)	Parent ions*	Mass error (ppm)	MS/MS determining fragments
O ₂ -dependent disso	ciation deriv	red products				
Epoxyallylic hydroperoxides	LA	12(13)-epoxy–9-hydroperoxy- octadeca10-enoic acid (12(13)-Ep,9- HPOME)	7.13; 7.31	327.2193 ; 309.2087; 291.1981	4.90	125.10; 139.11; 171.10
	ALA	12(13)-epoxy-9-hydroperoxy- octadeca-10,15-dienoic acid (12 (13)-Ep,9-HPODE)	5.47	325.2036 ; 307.1930	2.39	125.10; 97.07
		9(10)-epoxy-13-hydroperoxy- octadeca-11,15-dienoic acid (9(10)- Ep,13-HPODE)	6.02	325.2039 ; 307.1932	2.94	183.01; 197.12
Epoxyallylic ketones	LA	12(13)-epoxy–9-oxo-octadeca–10- enoic acid (12(13)-Ep,9-OxoOME)	8.61; 9.08	309.2088	4.90	171.10; 139.11; 127.11
	ALA	12(13)-epoxy-9-oxo- octadeca-10,15-dienoic acid (12 (13)-Ep,9-OxoODE)	6.78	307.1931		137.10; 125.10
Hydroperoxide ison	nerase-deriv	ed products				
Epoxy alcohols	LA	12(13)-epoxy–11-hydroxy- octadeca–9-enoic acid (12(13)- Ep,11-HOME)	4.94–6.35	311.2238	3.52	113.10; 169.12; 197.12; 211.13
	ALA	12(13)-epoxy-11-hydroxy- octadeca-9,15-dienoic acid (12(13)- Ep,11-HODE)	3.91;4.46; 4.83	309.2087	2.7	197.12; 111.08;169.12
		9(10)-epoxy-11-hydroxy- octadeca-12,15-dienoic acid (9(10)- Ep,11-HODE)	4.15:4.62	309.2089	2.24	171.10; 137.10
Ketones	LA	13-oxo-9Z,11E-octadecadienoic acid (13-oxoODE)	14.05	293.2134	4.17	113.10; 195.14
	ALA	9-oxo-octadeca-10,12,15-trienoic acid (9-Oxo-OTrE)	10.33	291.1978	2.37	111.08; 195.14
		13-oxo-9Z,11E,15Z-octadecatrienoic acid (13-Oxo-OTrE)	10.05	291.1976	2.13	121.10; 185.12
Double dioxygenat	-					
di-hydroperoxides	ALA	9,16-dihydroperoxy- octadeca–10,12,14-trienoic acid (9,16-diHPOTrE)	2.16; 2.44	341.1984; 323.1878 ; 305.1772; 287.1666	2.50	171.10; 97.06; 135.08; 109.06; 83.05; 57.03
Hydroperoxy- ketones	ALA	16-oxo, 9-HPOTrE or 9-oxo,16- HPOTrE	3.03	323.1872; 305.1766; 287.1661	1.90	135.08; 109.06; 171.10; 83.05; 57.03
di-ketone	ALA	9,16-oxo-octadeca-10,12,14-trienoic acid (9,16-diOxo-OTrE)	3.29	305.1768 ; 287.1662	1.99	171.88; 135.08; 83.05; 57.03
Reduced products						
Hydroxides	LA	13-hydroxy–9 <i>Z,11E</i> -octadecadienoic acid (13-HODE)	11.46	295.2287	2.71	195.14: 113.10
	ALA	9-hydroxy- <i>10E</i> ,12 <i>Z</i> ,15 <i>Z</i> -octadecadienoic acid (9-HOTrE)	8.20	293.2138	2.62	171.10; 121.10
		3-hydroxy-9Z,11E,15Z- octadecatrienoic acid (13-HOTrE)	8.70	293.2138	2.68	195.14
Elongated products C ₂₃ H ₃₈ O ₂	ALA	Unknown	39.99–42.30	345.2812	2.41	-

^{*} the parent ion of the MS/MS fragments shown is indicated in bold

Docking of the substrates at the binding pocket of Ma-LOX

To visualize how the substrates bind within the substrate binding pocket of Ma-LOX and to confirm the experimental results regarding regioselectivity, structural modelling of Ma-LOX and substrate docking was conducted. The PUFA substrates were docked in the substrate binding pocket of the Alphafold model of Ma-LOX (Fig. 5A). The selected docking poses for different PUFA substrates are shown in Fig. 5B and the docking parameters of those selected poses are listed in Table S6. The Alphafold model of Ma-LOX indicated that this enzyme possesses a shallower substrate-binding pocket compared to that of Cyanothece sp. LOX (Fig. S12). Based on structural comparison and prior reports describing alternative oxygen-access routes in LOXs [62], it is plausible that the shallower pocket of Ma-LOX may allow oxygen access not only through the putative oxygen channel but also partially from the substrate entrance (Fig. 5A,B). The substrate carbon atoms where hydrogen abstraction occurs are in close proximity to the iron (i.e., 4.1-7.8 Å), and the carbon atoms where the dioxygen insertion occurs are close to either the putative oxygen access channel or the substrate entrance. The docking results also suggested that most of the PUFAs preferred to enter the substrate binding pocket via a methyl end-first orientation (tail-first), except for DHA. LA and ALA showed the highest affinity to the substrate binding pocket by giving the lowest S-score (Table S6), in agreement with these being the preferred substrates.

To gain insight into how the 9,16-dihydroperoxide product forms when Ma-LOX uses ALA as a substrate, we conducted docking studies of 9-HPOTrE and 16-HPOTrE in the substrate-binding pocket of the Alphafold model of Ma-LOX. The docking parameters for the selected poses are listed in Table S6. The results, depicted in Fig. 5C, indicate that both 9-HPOTrE and 16-HPOTrE bind to the substrate-binding pocket with a methyl end-first orientation, allowing for second dioxygenation to occur at $\Delta 16$ on 9-HPOTrE via oxygen insertion from the putative oxygen channel and at $\Delta 9$ on 16-HPOTrE via oxygen insertion from the substrate entrance.

R. Chrisnasari et al. New BIOTECHNOLOGY 91 (2026) 36-51

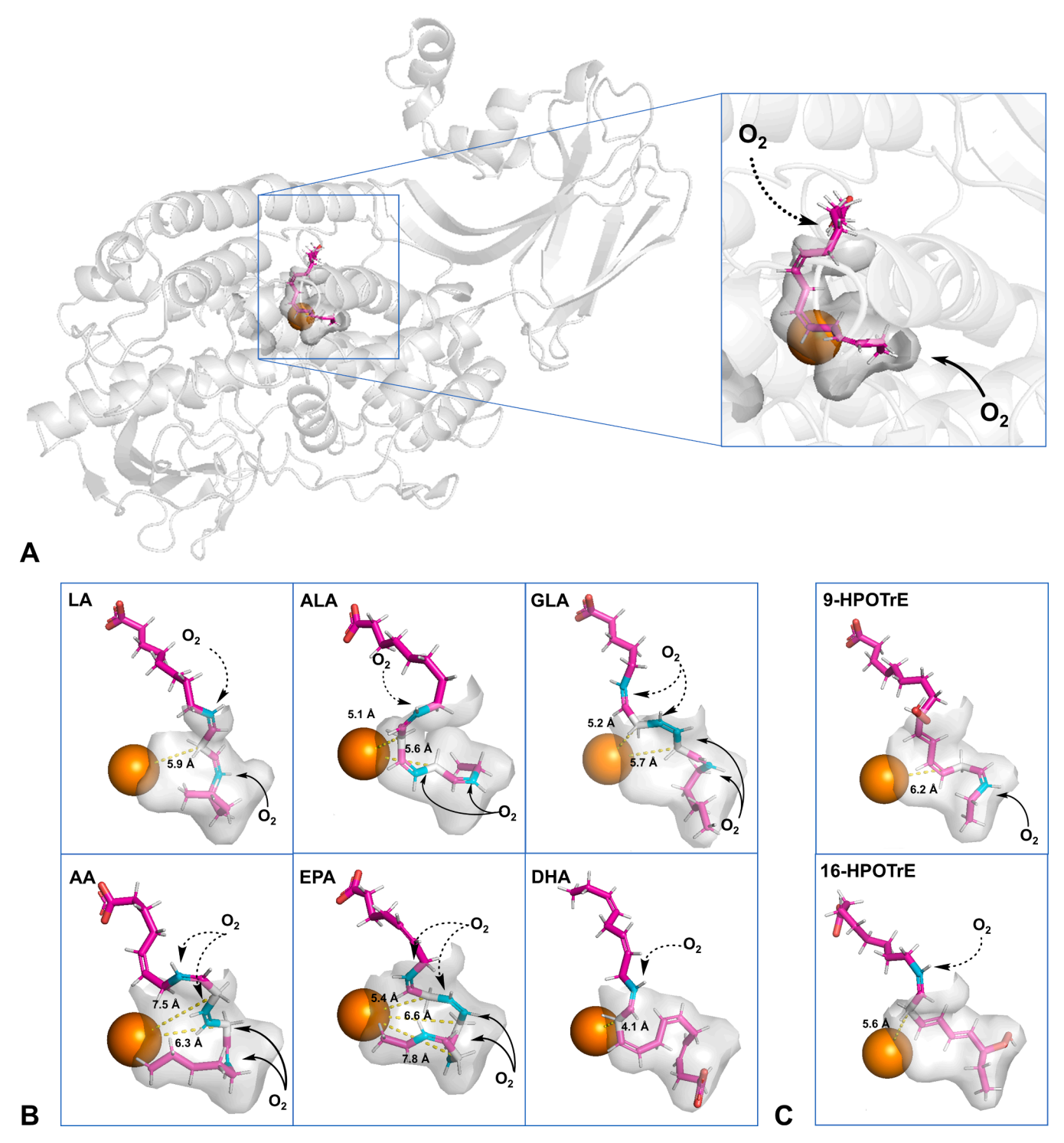


Fig. 5. Structural modeling of Ma-LOX and docking of PUFA substrates into the enzyme's binding pocket. (A) The three-dimensional structure of Ma-LOX was predicted using AlphaFold2. The catalytic iron, represented as an orange sphere, was positioned within the active site before docking PUFA substrates. Substrates (magenta sticks) were docked into the enzyme's binding cavity (light grey) using MOE 2022.02. (B) Docking conformations of six different PUFAs and (C) two HPOTrE regioisomers are displayed within the binding pocket. Black solid arrows indicate the proposed directions of oxygen insertion via the putative oxygen channel, while black dashed arrows represent oxygen insertion pathways from the substrate entry site. Carbon atoms involved in hydrogen abstraction are marked in white, and those where dioxygen insertion occurs are shown in cyan. Yellow dashed lines represent distances between the hydrogen abstraction sites and the iron center.

Discussion

Biochemical properties and substrate preference of Ma-LOX

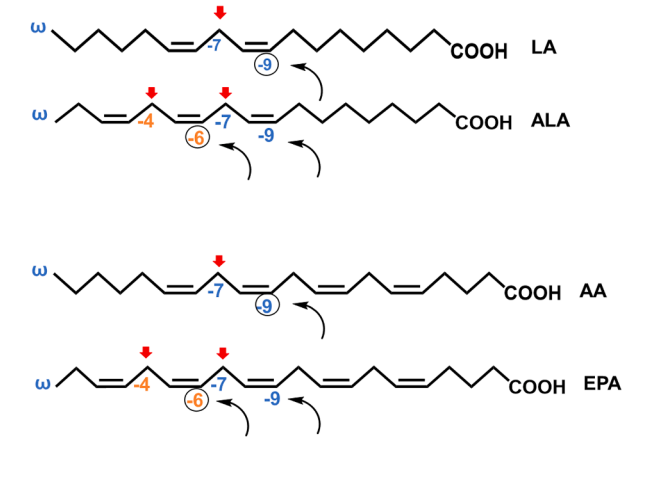
Exploration and characterization of new bacterial LOXs are

important to fully harness their potential in a wide range of applications. The present work focuses on the characterization of a LOX from *M. aeruginosa*, specifically its biochemical characteristics, optimal reaction conditions, substrate preference, and product profiles. Biochemical characterization of Ma-LOX revealed that, in solution, this enzyme

exists as a homodimer with an approximate subunit molecular mass of 75 kDa. This subunit size is comparable to that of *Cyanothece* sp. LOX (76.5 kDa), which belongs to the same phylogenetic cluster of bacterial LOXs [36]. Dimeric forms of LOX have been reported for various sources, including animal LOXs [63–66], fungal LOXs [67–69], and bacterial LOXs [34,70]. The purified Ma-LOX had an iron load of 76 %, indicating that it primarily utilizes iron as the catalytic cofactor. Although manganese was below the detection limit in our ICP-MS analysis, previous studies have reported that some bacterial LOXs can incorporate either Fe or Mn into their active sites [34,71]. Therefore, the remaining fraction of enzyme molecules may contain Mn or exist as apoenzyme (metal-free form). Comparable iron loads have been observed in other overexpressed bacterial LOXs [30,34,37,71,72]. Slight variations in iron loads among bacterial LOXs may result from differences in overexpression systems, growth conditions, or iron affinity.

The highest dioxygenation activity of Ma-LOX was observed between pH 5.0 and 7.0 and at 30 °C. The optimum conditions, around neutral pH and moderate temperature, are similar to the environmental conditions of *M. aeruginosa* from which the enzyme originated [73]. Evaluation of the substrate preference of Ma-LOX indicated that the enzyme prefers shorter-chain substrates (C18) over longer-chain (C20 and C22) and more unsaturated substrates, with GLA as an exception. GLA has the same chain length as LA and ALA, as well as the same number of double bonds as ALA; however, the enzyme showed significantly lower activity towards GLA. These results suggest that factors beyond the chain length and the number of double bonds of the substrate play a role in determining enzyme activity, such as the position of double bonds and their interaction with the binding pocket. This highlights the complex multifactorial determinants of LOX substrate preference.

Reported regioselectivity in Cyanothece sp. LOX



Hydrogen abstraction

Ma-LOX dioxygenation regioselectivity suggests O₂ insertion via two distinct pathways

Regioselectivity is a key characteristic of LOXs, as the location of the hydroperoxide group within FAHPs influences the biological and chemical properties of their downstream products. Ma-LOX exhibited a pronounced preference for oxygen insertion at the ω -5 position in LA, ALA, GLA, and AA. The enzyme exhibited the lowest regioselectivity with EPA, favoring the ω -2 position. For DHA, Ma-LOX preferred dioxygenation at the ω -8 position, with reduced activity at the ω -2 position. Due to its long chain and large number of (cis) double bonds, DHA theoretically has more potential sites for hydrogen abstraction or oxygen insertion. However, the twisted and rigid structure of DHA, as confirmed by docking results (Fig. 5B), limits the available sites for these reactions, resulting in fewer observed dioxygenation sites.

To better understand how FAHPs derived from various PUFAs are formed, we illustrate the positioning of carbon atoms for hydrogen abstraction and oxygen insertion, as previously reported for Cyanothece sp. LOX [36] and observed here for Ma-LOX (Fig. 6). The figure depicts the regio-specific abstraction of bis-allylic hydrogens and subsequent oxygenation at defined carbon positions along the PUFA backbone, highlighting how differences in substrate chain length and double-bond configuration influence the preferred dioxygenation sites. In general, the reaction is initiated by the ferric iron at the active site, which abstracts a hydrogen atom from the central carbon of a pentadiene moiety within the substrate [74]. The resulting substrate radical can delocalize the unpaired electron to either the [+2] or [-2] position relative to the site of hydrogen abstraction. This is followed by the insertion of molecular oxygen, forming a fatty acid peroxyl radical. The peroxyl radical is then reduced by an electron donated from the ferrous iron and subsequently protonated, yielding the corresponding FAHP [74-76]. The regioselectivity of dioxygen insertion is ultimately influenced not only by the

Regioselectivity observed in Ma-LOX

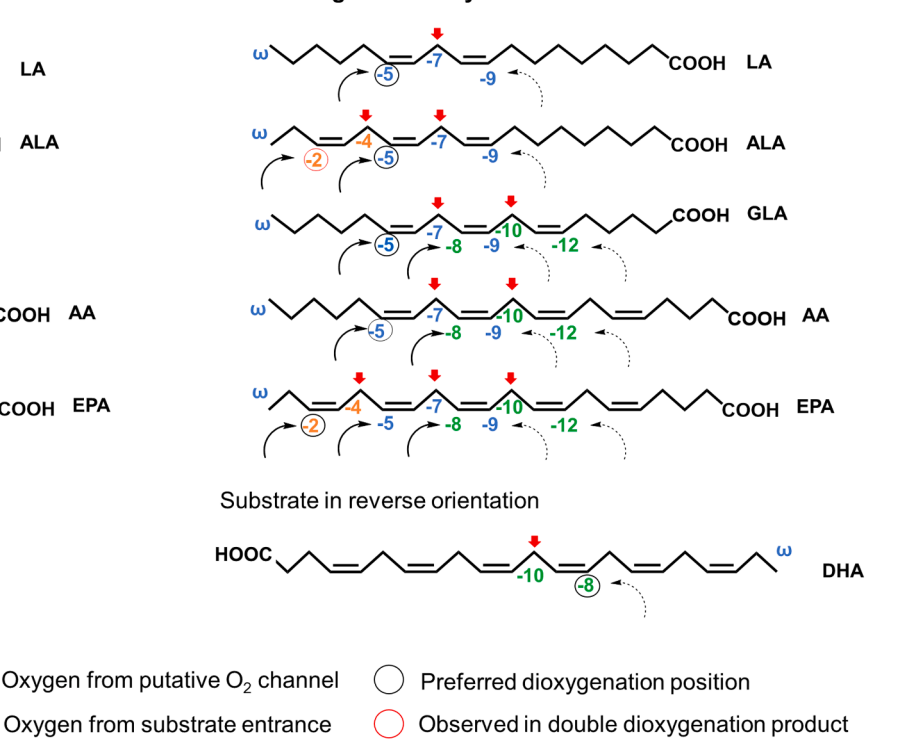


Fig. 6. Illustration of carbon atom positions for the hydrogen abstraction and the oxygen insertion in *Cyanothece* sp. LOX (left panel) [36] and Ma-LOX (right panel), counted from the methyl-end (ω). The carbon atoms where hydrogen abstraction occurred (indicated by red arrows) and the subsequent dioxygenation observed, [+2] and/or the [-2] positions, are indicated in the same color, i.e., green, blue or orange. The most preferred dioxygenation positions are shown in black circles, while the dioxygenation position observed only in the double dioxygenation product is shown in red circle. The proposed oxygen directions from the putative O_2 channel are shown by the direction of the black-line arrows, while those from the substrate entrance are shown by the black-dotted arrows.

location of the carbon radical but also by the size and direction of the oxygen access channel that directs the oxygen molecule to the enzyme's active site [45–47].

Cyanothece sp. LOX has been reported to exhibit regioselectivity at the ω -9 position on LA and AA, and regioselectivity at both ω -9 and ω -6 positions on ALA and EPA (Fig. 6 left panel) [36]. This observed regioselectivity in Cyanothece sp. LOX suggests that hydrogen abstraction occurs at two different positions on ALA and EPA, while only at one position on LA and AA. However, in all cases, the dioxygenation only occurs at the [-2] position from the abstracted hydrogen, suggesting that the oxygen molecule enters from one direction, specifically from the carboxyl-end of the substrate. In comparison, Ma-LOX catalyzes the hydrogen abstraction at multiple sites on PUFAs with more than two double bonds, resulting in different regioselectivities (Fig. 6 right panel). The variations in regioselectivity among different PUFAs suggest that dioxygen molecules might be inserted from two different directions, i.e., from the carboxyl- and the methyl-end of the substrate, as indicated by the direction of the black-dotted arrows and the black-line arrows, respectively (Fig. 6 right panel). The hypothesis that oxygen is inserted from two different directions is supported by the shallower substrate binding pocket observed in the Alphafold model of Ma-LOX compared to that of Cyanothece sp. LOX (Fig. S12). The shallower pocket of Ma-LOX may facilitate oxygen insertion from both the putative oxygen channel and the substrate entrance as suggested by the docking results (Fig. 5). The oxygen insertion via the oxygen channel has been reported before [23,45-47], however, oxygen insertion via the substrate entrance is reported here for the first time.

A recent study using molecular dynamics simulations reported the presence of two primary oxygen channels based on conserved motifs and helical structures across the LOX family, including plants, mammals, and bacteria [62]. We also identified these two conserved motifs and structures in the Ma-LOX sequence and model (Fig. S13), which align with the expected direction of oxygen flow (Fig. 5A). This observation supports our hypothesis that dioxygen molecules can enter the enzyme's active site from two different directions—via both the putative oxygen channel and the substrate entrance. Furthermore, this finding highlights the role of Ma-LOX's shallower substrate-binding pocket in its unique dioxygenation pattern observed in different PUFAs (Fig. 6), as this unique pattern is not observed in other LOXs.

In addition, compared to the regioselectivity observed in *Cyanothece* sp. LOX [36], Ma-LOX showed a preference for dioxygenation positions closer to the methyl-end. The larger amino acid residues that are present at the bottom of the substrate binding pocket (i.e., F367 and M408), compared to those in *Cyanothece* sp. LOX (Fig. 2B) provide a less spacious binding pocket, allowing the substrate to enter less deeply. Consequently, Ma-LOX prefers to add a hydroperoxyl group closer to the methyl-end than *Cyanothece* sp. LOX.

R-enantioselectivity of Ma-LOX

Ma-LOX exhibits pronounced R-enantioselectivity, specifically converting LA to 13R-HPODE (Fig. 3C). This enantioselectivity is a distinctive feature shared by other bacterial lipoxygenases (LOXs) within the same phylogenetic cluster [35], including those from Cyanothece sp. [36], Nostoc sp. PCC 7120 [39], and Acaryochloris marina [38]. The consistent production of R-hydroperoxides across these enzymes underscores a conserved property determining enantioselectivity unique to this group of bacterial LOXs. Understanding the structural basis for this R-selectivity is crucial, as it may reveal novel catalytic strategies distinct from those of plant or mammalian LOXs, which predominantly produce S-enantiomers. Elucidating the molecular determinants underlying this rare enantioselectivity will also enable efficient, sustainable biosynthesis of enantiomerically pure R-type oxylipins, compounds of growing interest for pharmaceutical applications [5,7]. However, such investigations are beyond the scope of the present study.

O₂-dependent dissociation- and HPI-derived products formation

In addition to examining the primary dioxygenase activity of Ma-LOX, we explored the formation of secondary products in Ma-LOXcatalyzed reactions. Analyzing and identifying these secondary products offers important insights into the enzyme's mechanisms and its full catalytic potential. The results revealed that both secondary products derived from O₂-dependent dissociation (i.e., epoxyallylic hydroperoxides and epoxyallylic ketones) and HPI activity (i.e., epoxy alcohols and ketones) were observed when using LA and ALA as substrates. The presence of HPI activity in Ma-LOX was further confirmed by the increase of epoxy alcohols and decrease of FAHPs when increasing the enzyme concentration (Fig. S10). The rise in enzyme concentration increased the amount of ferrous enzyme (LOX-Fe2+) that is active towards FAHP. Through HPI activity, FAHP is converted into epoxy alcohol, and the enzyme reverts to its ferrous form, allowing a continuous cycle of epoxy alcohol formation. However, increasing the incubation time did not significantly increase the formation of epoxy alcohols (Fig. S11), consistent with our recent observation in another bacterial LOX from Burkholderia thailandensis [77]. This suggests that after a certain period, the enzyme ceases its HPI activity. One explanation could be that the ferrous enzyme (LOX-Fe²⁺) is oxidized to its free ferric form (LOX-Fe³⁺-OH), causing it to escape the HPI cycle (Fig. 1). The escape of the enzyme from the HPI cycle is supported by the presence of epoxyallylic hydroperoxides, which are products of O2-dependent dissociation. Alternatively, the enzyme may gradually lose its activity during longer incubation times, suggesting a time-dependent stability that could be optimized in future experiments.

Formation of double dioxygenation products and their derivatives

In addition to O2-dependent dissociation- and HPI-derived secondary products, Ma-LOX also produced double dioxygenation products and their derivatives from ALA. The proposed mechanism for the formation of these products is depicted in Fig. 7. When ALA is used as a substrate, hydrogen abstraction occurs at either the $\Delta 11$ or $\Delta 14$ carbon atom, which theoretically allows oxygen insertion at the $\Delta 9$, $\Delta 12$, $\Delta 13$, or $\Delta 16$ positions. Oxygen insertion at the $\Delta 12$ position was not observed, and oxygen insertion at the $\Delta 9$ position was observed to a minor extent (1.7 % of total single dioxygenation products) (Table S3). The absence of dioxygenation at the $\Delta 12$ position likely results from poor oxygen access, as supported by docking results shown in Fig. 5B (panel ALA). The low dioxygenation observed at the $\Delta 9$ position may be due to limited oxygen access, supported by docking results indicating that position $\Delta 9$ is only accessible via the substrate entrance (Fig. 5B, panel ALA). Moreover, the oxygenated product at the $\Delta 9$ position may undergo a second dioxygenation, as one of the two original pentadiene moieties remains intact, forming 9,16-diHPOTrE.

On the other hand, the main product of the ALA reaction 13-HPOTrE (Table S3) cannot undergo a second dioxygenation because the oxygen insertion at the $\Delta13$ position disrupts both conjugated pentadiene systems in the substrate. In contrast, oxygen insertion at the $\Delta16$ position preserves one pentadiene moiety, thereby allowing a second dioxygenation to occur. Structural modeling indicates that the $\Delta16$ carbon is accessible through the same oxygen channel used for insertion at $\Delta13$ (Fig. 5B, panel ALA), making dioxygenation at $\Delta16$ mechanistically feasible. The absence of detectable 16-HPOTrE among the primary products supports this interpretation, suggesting that it is rapidly converted to 9,16-diHPOTrE through a subsequent oxygenation step.

The derivatives of the double dioxygenation product, 9,16-diH-POTrE, are formed when this product enters the HPI cycle, producing either 16-oxo-9-HPOTrE or 9-oxo-16-HPOTrE. These compounds can then re-enter the HPI cycle, ultimately forming 9,16-dioxo-OTrE (Fig. 7). However, it is possible that the reaction sequence proceeds differently. For instance, the products of the first dioxygenation, 9-HPOTrE and 16-HPOTrE, may enter the HPI cycle to produce their corresponding epoxy

Fig. 7. Proposed mechanism for the formation of double dioxygenation products from ALA and its derivatives by hydroperoxide isomerase activity of Ma-LOX. The carbon atoms where hydrogen abstraction (indicated by red arrows) and the subsequent dioxygenation occurred, counted from the carboxyl end, are indicated in the same color, i.e., blue or orange. The proposed oxygen directions are shown by black curved arrows.

alcohols and ketones. It is possible that only the ketones undergo a second dioxygenation, yielding either 16-oxo-9-HPOTrE or 9-oxo-16-HPOTrE. These products then re-enter the HPI cycle, forming 9,16-dioxo-OTrE. In both cases, the preference for the formation of ketones rather than epoxy alcohols by HPI activity in this double dioxygenation product remains poorly understood.

The hydrogen abstraction at the $\Delta14~(\omega\text{-}4)$ position and the subsequent oxygen insertion at the $\Delta16~(\omega\text{-}2)$ position in ALA are consistent with the observations in other $\omega3\text{-PUFA}$ substrates, i.e., EPA and DHA (Fig. 3). Unlike what is observed in ALA, the double dioxygenation reaction was barely seen in the other $\omega3\text{-PUFAs}$ due to the low activity towards them. The double dioxygenation was also not observed when using LA because it loses its pentadiene moiety upon the first dioxygenation.

Despite recent reports of double dioxygenation activity in bacterial LOX [32,40–42], the mechanisms underlying this activity remain poorly understood. Previously, the double dioxygenation reaction was explained by the concept of different substrate orientations upon entering the binding pocket. For example, in soybean LOX-1 with arachidonic acid (AA), this leads to the formation of 5,15-di-HPETE and 8,15-di-HPETE [78]. In this scenario, the initial product, 15-HPETE, re-enters the enzyme in a carboxyl end-first (head-first) orientation and undergoes a second dioxygenation at positions $\Delta 5$ or $\Delta 8$, producing double dioxygenation products. The second dioxygenation at these positions represents a shift of 1 or 2 carbon atoms relative to the original dioxygenation position when the substrate is oriented tail-first. However, in the case of Ma-LOX, this scenario may not apply. For a possible head-first orientation, the dioxygenation occurs at the ninth carbon atom, counting from the carboxylic acid group. In contrast, for a tail-first orientation, the dioxygenation occurs at either the third or sixth carbon atom, counting from the methyl group. This represents a shift of 6 or 3 carbon atoms, which is significantly larger than what is observed in soybean LOX-1. Moreover, docking results for 9-HPOTrE and 16-HPOTrE indicate that these molecules bind to the substrate-binding pocket in a tail-first orientation, similar to that of ALA during the first dioxygenation event (Fig. 5C).

The double dioxygenation reaction was also explained by different penetration depths of the substrate in Sphingopyxis macrogoltabida LOX, which catalyzes the synthesis of 9S,15S- and 11S,17S-dihydroperoxy fatty acids from C20 and C22 PUFAs [32]. In this case, the enzyme initially dioxygenates at $\Delta 9$ to produce 9-HPETE from AA. Subsequently, 9-HPETE re-enters the binding pocket, giving a second dioxygenation at $\Delta 15$, as the hydroperoxide group at $\Delta 9$ hinders further penetration of the substrate [32]. If this scenario applies to what is observed in Ma-LOX, for instance, when the first dioxygenation occurs at the $\Delta 9$ position, the hydroperoxide group at this position hinders further penetration of the substrate, resulting in the second dioxygenation at the $\Delta 16$ position. By the same principle, when the first dioxygenation occurs at the $\Delta 16$ position, the hydroperoxide group should inhibit the entry of the substrate into the binding pocket, as the hydroperoxide position is almost at the methyl-end. Consequently, the accumulation of 16-HPOTrE should be detected. However, accumulation of 16-HPOTrE was not observed, indicating that this scenario may not apply for Ma-LOX.

In the case of Ma-LOX, we hypothesize that its shallow binding pocket (Fig. S12) allows the insertion of oxygen via two directions: the substrate entrance and the putative oxygen channel, leading to the formation of double dioxygenation product 9,16-diHPOTrE. When the first dioxygenation occurs at the $\Delta16$ position producing 16-HPOTrE, the hydroperoxide group at this position hinders the insertion of oxygen from the putative oxygen channel. As a consequence, dioxygenation at the $\Delta13$ position is not possible; instead, the oxygen insertion from the

substrate entrance to the $\Delta 9$ position occurs (Fig. 8A). The docking of 16-HPOTrE confirmed that this molecule binds to the substrate binding pocket with a tail-first orientation, allowing a second dioxygenation to occur at the $\Delta 9$ position via the substrate entrance (Fig. 5C). On the other hand, when first dioxygenation occurs at the $\Delta 9$ position, the hydroperoxide group at this position hinders the insertion of oxygen from the substrate entrance, thus the dioxygenation at $\Delta 12$ is not possible. However, oxygen insertion from the putative oxygen channel to the $\Delta 16$ position is still possible (Fig. 8B). The docking of 9-HPOTrE suggested that this molecule binds to the substrate binding pocket with a tail-first orientation, allowing a second dioxygenation to occur at the $\Delta 16$ position via the putative oxygen channel (Fig. 5C). In both scenarios, the final product is 9,16-diHPOTrE. For the first time, this mechanism underlying double dioxygenation activity, facilitated by the shallow shape of the substrate-binding pocket, is proposed for a LOX.

Formation of elongated products

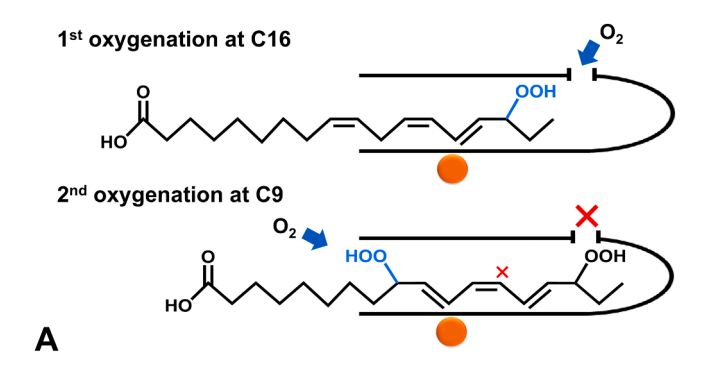
In addition to the double dioxygenation product and its derivatives, Ma-LOX also produced elongated products with the chemical formula of C₂₃H₃₈O₂, which elute at RT 39.60-41.78 (Fig. 4B). The formation of C23 compounds from C18 substrate molecules indicates the occurrence of combined decomposition and coupling reactions. Previous studies have reported that ferrous ions or anaerobic conditions accelerates the decomposition of FAHPs through homolytic cleavage yielding ferric ions, hydroxide ions, and alkoxy radicals [15,79]. In the case of 13-HPODE, the alkoxy radical then undergoes β-scission to form pentane in the presence of any suitable hydrogen donor [15,79]. The main FAHP product of Ma-LOX from ALA, 13-γHPOTrE, may undergo a similar decomposition generating pentene. Possibly, the resulting pentene reacts with either ALA or HOTrE, forming a C23 compound, as such coupling has been reported before under anaerobic conditions [8,80]. In our experiment, we use a closed system, and the available oxygen is utilized for dioxygenation, double dioxygenation, and O2-dependent dissociation reactions. As the oxygen level depletes, the homolytic cleavage and coupling reactions may occur. However, the exact mechanism for the formation of the elongated products in the enzymatic reaction of Ma-LOX is not fully clarified.

Conclusion

The study of bacterial LOXs holds substantial significance due to their distinct biochemical properties and potential for a wide range of applications. In this work, we characterized the biochemical properties and product profiles of a novel lipoxygenase from M. aeruginosa (Ma-LOX). Our findings indicate that Ma-LOX predominantly forms a homodimer, exhibiting optimal enzymatic activity within a pH range of 5.0–7.0 and at 30°C. The enzyme demonstrated a pronounced substrate preference for LA and ALA, with dioxygenation occurring predominantly at the ω-5 position. Ma-LOX exhibited high enantioselectivity, favoring the formation of 13R-HPODE from LA. Notably, Ma-LOX exhibited a unique regioselectivity pattern, where oxygen insertion appears to occur from both the putative oxygen channel and the substrate entry site, likely a consequence of its shallow substrate-binding pocket. We propose that this structural feature also facilitates Ma-LOX's double dioxygenation activity, a novel mechanism not previously reported for LOXs. Furthermore, Ma-LOX displayed atypical HPI activity, resulting in the production of epoxy alcohols and ketones. Collectively, these findings underscore the catalytic versatility of Ma-LOX and suggest promising directions for future research aimed at exploiting its enzymatic properties for industrial and biotechnological applications.

CRediT authorship contribution statement

Ruth Chrisnasari: Writing – review & editing, Writing – original draft, Visualization, Validation, Methodology, Investigation, Formal



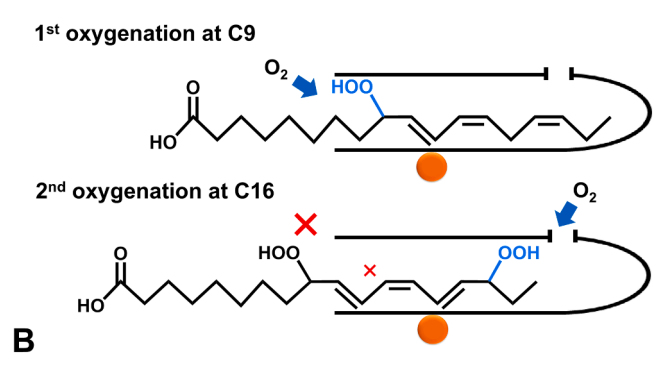


Fig. 8. Illustration of double dioxygenation product formation from ALA by Ma-LOX. A. First dioxygenation at the $\Delta 16$ position prevents further dioxygenation at $\Delta 13$ and favoring insertion at $\Delta 9$ via the substrate entrance. B. First dioxygenation at $\Delta 9$ hinders further insertion at $\Delta 12$, instead allowing dioxygenation at $\Delta 16$ via the oxygen channel.

analysis, Data curation, Conceptualization. Shuyue Chen: Visualization, Investigation, Formal analysis, Data curation. Tom A. Ewing: Writing – review & editing, Supervision, Conceptualization. Marie Hennebelle: Writing – review & editing, Supervision, Conceptualization. van Berkel Willem J. H.: Writing – review & editing, Supervision. Jean-Paul Vincken: Writing – review & editing, Supervision. Roelant Hilgers: Writing – review & editing, Supervision. Daan van Vliet: Investigation, Formal analysis, Data curation.

Funding

This research was funded by the Indonesian Endowment Fund for Education (LPDP), Ministry of Finance of the Republic of Indonesia, through a doctoral scholarship awarded to Ruth Chrisnasari (Grant No. 0006605/BIO/D/BUDI-2019).

Declaration of Competing Interest

The authors have no interest statement to declare.

Acknowledgment

The authors express their sincere gratitude to Prof. Marco W. Fraaije and Dr. Hein J. Wijma (University of Groningen) for conducting the structural modeling of *M. aeruginosa* LOX and generating its AlphaFold2 structure. We also thank Mark Sanders for his support during UHPLC-MS method development and Thore Diefenbach for his help for SEC analysis. Appreciation is extended to Michal Zatorski for his contributions to the preliminary activity screening of bacterial LOX candidates. Part of this work was performed using a Thermo Scientific Q Exactive Focus Orbitrap MS system, provided by Shared Research Facilities—WUR and co-funded by the Province of Gelderland, The Netherlands.

Appendix A. Supporting information

Supplementary data associated with this article can be found in the online version at doi:10.1016/j.nbt.2025.11.005.

Data availability

Data will be made available on request.

References

- Casey R, Hughes RK. Recombinant lipoxygenases and oxylipin metabolism in relation to food quality. Food Biotechnol 2004;18:135–70. https://doi.org/ 10.1081/FRT-200025673
- [2] Liu C, Liu F, Cai J, Xie UW, Long TE, Turner SR, et al. Polymers from fatty acids: Poly(co-hydroxyl tetradecanoic acid) synthesis and physico-mechanical studies. ACS Symp Ser 2012;1105:131–50. https://doi.org/10.1021/BK-2012-1105. CH009.
- [3] Song JW, Jeon EY, Song DH, Jang HY, Bornscheuer UT, Oh DK, et al. Multistep enzymatic synthesis of long-chain α,ω-dicarboxylic and ω-hydroxycarboxylic acids from renewable fatty acids and plant oils. Angew Chem Int Ed 2013;52:2534–7. https://doi.org/10.1002/anje.201209187.
- [4] Blum M, Dogan I, Karber M, Rothe M, Schunck WH. Chiral lipidomics of monoepoxy and monohydroxy metabolites derived from long-chain polyunsaturated fatty acids. J Lipid Res 2019;60:135–48. https://doi.org/10.1194/ il-M080755
- [5] Isobe Y, Arita M, Iwamoto R, Urabe D, Todoroki H, Masuda K, et al. Stereochemical assignment and anti-inflammatory properties of the omega-3 lipid mediator resolvin E3. J Biochem 2013;153:355–60. https://doi.org/10.1093/jb/mvs151.
- [6] Ambaw YA, Fuchs D, Raida M, Mazengia NT, Torta F, Wheelock CE, et al. Changes of tear lipid mediators after eyelid warming or thermopulsation treatment for meibomian gland dysfunction. Prostaglandins Other Lipid Mediat 2020;151. https://doi.org/10.1016/j.prostaglandins.2020.106474.
- [7] Oh SF, Vickery TW, Serhan CN. Chiral lipidomics of E-series resolvins: Aspirin and the biosynthesis of novel mediators. Biochim Biophys Acta Mol Cell Biol Lipids 2011;1811:737–47. https://doi.org/10.1016/j.bbalip.2011.06.007.
- [8] Zheng Y, Brash AR. On the role of molecular oxygen in lipoxygenase activation: Comparison and contrast of epidermal lipoxygenase-3 with soybean lipoxygenase-1. J Biol Chem 2010;285:39876–87. https://doi.org/10.1074/jbc.M110.180794.
- [9] Schilstra MJ, Veldink GA, Vliegenthart JFG. Kinetic analysis of the induction period in lipoxygenase catalysis. Biochemistry 1993;32:7686–91. https://doi.org/ 10.1021/dxipoxyge1312.
- [10] Schilstra MJ, Veldink GA, Verhagen J, Vliegenthart JFG. Effect of lipid hydroperoxide on lipoxygenase kinetics. Biochemistry 1992;31:7692–9. https://doi.org/10.1021/bi00148a033.
- [11] Yu Z, Schneider C, Boeglin WE, Marnett LJ, Brash AR. The lipoxygenase gene ALOXE3 implicated in skin differentiation encodes a hydroperoxide isomerase. PNAS 2003;100:9162–7. https://doi.org/10.1073/pnas.1633612100.
- [12] Schilstra MJ, Veldink GA, Vliegenthart JFG. The dioxygenation rate in lipoxygenase catalysis is determined by the amount of Iron(III) lipoxygenase in solution. Biochemistry 1994;33:3974–9. https://doi.org/10.1021/bi00179a025.
- [13] de Groot JJMC, Garssen GJ, Veldink GA, Vliegenthart JFG, Boldingh J, Egmond MR. On the interaction of soybean lipoxygenase-1 and 13-Lhydroperoxylinoleic acid, involving yellow and purple coloured enzyme species. FEBS Lett 1975;56:50–4. https://doi.org/10.1016/0014-5793(75)80109-8.
- [14] Garssen GJ, Veldink GA, Vliegenthart JFG, Boldingh J. The formation of threo-11-hydroxy-trans-12: 13-epoxy-9-cis-octadecenoic acid by enzymic isomerisation of 13-l-hydroperoxy-9-cis,11-trans-octadecadienoic acid by soybean lipoxygenase-1. Eur J Biochem 1976;62:33–6. https://doi.org/10.1111/j.1432-1033.1976. b110094.x.
- [15] Garssen GJ, Vliegenthart JFG, Boldingh J. An anaerobic reaction between lipoxygenase, linoleic acid and its hydroperoxides. Biochem J 1971;122:327–32. https://doi.org/10.1042/bj1220327.
- [16] Cristea M, Oliw EH. A G316A mutation of manganese lipoxygenase augments hydroperoxide isomerase activity: Mechanism of biosynthesis of epoxyalcohols. J Biol Chem 2006;281:17612–23. https://doi.org/10.1074/jbc.M510311200.
- [17] Yadav JS, Somaiah R, Ravindar K, Chandraiah L. Stereoselective total synthesis of (+)-mueggelone, a novel inhibitor of fish development. Tetrahedron Lett 2008;49: 2848–50. https://doi.org/10.1016/j.tetlet.2008.02.022.
- [18] Yadav JS, Srinivas Dale. Titanocene induced deoxygenation of di-epoxides a convenient regioselective preparation of 1,3-diols. Chem Lett 1997;CL-970345: 905-6. https://doi.org/10.1246/cl.1997.905.
- [19] Riera A, Moreno M. Synthetic applications of chiral unsaturated epoxy alcohols prepared by sharpless asymmetric epoxidation. Molecules 2010;15:1041–73. https://doi.org/10.3390/molecules15021041.
- [20] Rodríguez A, Nomen M, Spur BW, Godfroid JJ, Lee TH. Total synthesis of leukotrienes from butadiene. Eur J Org Chem 2000:2991–3000. https://doi.org/ 10.1002/1099-0690(200009)2000:17<2991::AID-EJOC2991>3.0.CO:2-H.
- [21] Brash AR. Lipoxygenases: Occurrence, functions, catalysis, and acquisition of substrate. J Biol Chem 1999;274:23679–82. https://doi.org/10.1074/ jbc.274.34.23679.
- [22] Brash AR. Lipoxygenases: A chronological perspective on the synthesis of S and R fatty acid hydroperoxides. Bioactive Lipid Mediators: Current Reviews and

- Protocols. Springer Japan; 2015. p. 69–84. https://doi.org/10.1007/978-4-431-55660.5.5
- [23] Newcomer ME, Brash AR. The structural basis for specificity in lipoxygenase catalysis. Protein Sci 2015;24:298–309. https://doi.org/10.1002/pro.2626.
- [24] Coffa G, Schneider C, Brash AR. A comprehensive model of positional and stereo control in lipoxygenases. Biochem Biophys Res Commun 2005;338:87–92. https:// doi.org/10.1016/j.bbrc.2005.07.185.
- [25] Ivanov I, Kuhn H, Heydeck D. Structural and functional biology of arachidonic acid 15-lipoxygenase-1 (ALOX15). Gene 2015;573:1–32. https://doi.org/10.1016/j. gene.2015.07.073.
- [26] Kuhn H, Banthiya SS, Van Leyen K, Leyen K van. Mammalian lipoxygenases and their biological relevance. Biochim Biophys Acta 2015;1851:308–30. https://doi. org/10.1016/j.bbalip.2014.10.002.
- [27] Kuhn H, Saam J, Eibach S, Holzhütter HG, Ivanov I, Walther M. Structural biology of mammalian lipoxygenases: Enzymatic consequences of targeted alterations of the protein structure. Biochem Biophys Res Commun 2005;338:93–101. https:// doi.org/10.1016/j.bbrc.2005.08.238.
- [28] Zhuravlev A, Gavrilyuk V, Chen X, Aksenov V, Kuhn H, Ivanov I. Structural and functional biology of mammalian ALOX isoforms with particular emphasis on enzyme dimerization and their allosteric properties. Int J Mol Sci 2024;25. https:// doi.org/10.3390/ijms252212058.
- [29] Li S, Hou S, Sun Y, Sun M, Sun Y, Li X, et al. Genome-wide identification and expression analysis under abiotic stress of the lipoxygenase gene family in maize (Zea mays). Genes (Basel) 2025;16. https://doi.org/10.3390/genes16010099.
- [30] Banthiya S, Kalms J, Galemou Yoga E, Ivanov I, Carpena X, Hamberg M, et al. Structural and functional basis of phospholipid oxygenase activity of bacterial lipoxygenase from *Pseudomonas aeruginosa*. Biochim Biophys Acta Mol Cell Biol Lipids 2016;1861:1681–92. https://doi.org/10.1016/j.bbalip.2016.08.002.
- [31] Qi Y-K, Zheng Y-C, Zhang Z-J, Xu J-H. Efficient transformation of linoleic acid into 13(S)-hydroxy-9,11-(2,E)-octadecadienoic acid using putative lipoxygenases from Cyanobacteria. ACS Sustain Chem Eng 2020;8:5558–65. https://doi.org/10.1021/ acssuschemeng.9b07457.
- [32] Kim SE, Lee J, An JU, Kim TH, Oh CW, Ko YJ, et al. Regioselectivity of an arachidonate 9S-lipoxygenase from Sphingopyxis macrogoltabida that biosynthesizes 9S,15S- and 11S,17S-dihydroxy fatty acids from C20 and C22 polyunsaturated fatty acids. Biochim Biophys Acta Mol Cell Biol Lipids 2022;1867:159091. https://doi.org/10.1016/J.BBALIP.2021.159091.
- [33] Goloshchapova K, Stehling S, Heydeck D, Blum M, Kuhn H. Functional characterization of a novel arachidonic acid 12S-lipoxygenase in the halotolerant bacterium Myxococcus fulvus exhibiting complex social living patterns. Microbiol Open 2018;8:1–17. https://doi.org/10.1002/mbo3.775.
- [34] An JU, Hong SH, Oh DK. Regiospecificity of a novel bacterial lipoxygenase from Myxococcus xanthus for polyunsaturated fatty acids. Biochim Biophys Acta Mol Cell Biol Lipids 2018;1863:823–33. https://doi.org/10.1016/j.bbalip.2018.04.014.
- [35] Chrisnasari R, Hennebelle M, Vincken J-P, van Berkel WJH, Ewing TA. Bacterial lipoxygenases: Biochemical characteristics, molecular structure and potential applications. Biotechnol Adv 2022;61:108046. https://doi.org/10.1016/j. biotechadv.2022.108046
- [36] Newie J, Andreou A, Neumann P, Einsle O, Feussner I, Ficner R. Crystal structure of a lipoxygenase from *Cyanothece* sp. may reveal novel features for substrate acquisition. J Lipid Res 2016;57:276–86. https://doi.org/10.1194/JLR.M064980.
- [37] Chrisnasari R, Hennebelle M, Nguyen KA, Vincken J-P, van Berkel WJH, Ewing TA. Engineering the substrate specificity and regioselectivity of *Burkholderia* thailandensis lipoxygenase. N Biotechnol 2024;84:64–76. https://doi.org/10.1016/ i.pht 2024.09.007
- [38] Gao B, Boeglin WE, Brash AR. Omega-3 fatty acids are oxygenated at the n-7 carbon by the lipoxygenase domain of a fusion protein in the cyanobacterium Acaryochloris marina. Biochim Biophys Acta Mol Cell Biol Lipids 2010;1801:58–63. https://doi.org/10.1016/J.BBALIP.2009.09.004.
- [39] Andreou A, Vanko M, Bezakova L, Feussner I. Properties of a mini 9R-lipoxygenase from *Nostoc* sp. PCC 7120 and its mutant forms. Phytochemistry 2008;69:1832–7. https://doi.org/10.1016/j.phytochem.2008.03.002.
- [40] Lee J, An J-U, Kim T-H, Ko Y-J, Park J-B, Oh D-K. Discovery and engineering of a microbial double-oxygenating lipoxygenase for synthesis of dihydroxy fatty acids as specialized proresolving mediators. ACS Sustain Chem Eng 2022;8:16172–83. https://doi.org/10.1021/acssuschemeng.0c04793.
- [41] Oh CW, Kim SE, Lee J, Oh DK. Bioconversion of C20- and C22-polyunsaturated fatty acids into 95,155- and 115,175-dihydroxy fatty acids by Escherichia coli expressing double-oxygenating 9S-lipoxygenase from Sphingopyxis macrogoltabida. J Biosci Bioeng 2022;134:14-20. https://doi.org/10.1016/J.JBIOSC.2022.04.001.
- J Biosci Bioeng 2022;134:14–20. https://doi.org/10.1016/J.JBIOSC.2022.04.001.

 [42] Kim TH, Lee J, Kim SE, Oh DK. Biocatalytic synthesis of dihydroxy fatty acids as lipid mediators from polyunsaturated fatty acids by double dioxygenation of the microbial 12S-lipoxygenase. Biotechnol Bioeng 2021;118:3094–104. https://doi.org/10.1002/bit.27820.
- [43] Ishihara T, Yoshida M, Arita M. Omega-3 fatty acid-derived mediators that control inflammation and tissue homeostasis. Int Immunol 2019;31:559–67. https://doi. org/10.1093/INTIMM/DXZ001.
- [44] Basil MC, Levy BD. Specialized pro-resolving mediators: endogenous regulators of infection and inflammation. 2015 16:1 Nat Rev Immunol 2015;16:51–67. https://doi.org/10.1038/NRI.2015.4.
- [45] Coffa G, Brash AR. A single active site residue directs oxygenation stereospecificity in lipoxygenases: Stereocontrol is linked to the position of oxygenation. Proc Natl Acad Sci USA 2004;101:15579–84. https://doi.org/10.1073/pnas.0406727101.
- [46] Collazo L, Klinman JP. Control of the position of oxygen delivery in soybean lipoxygenase-1 by amino acid side chains within a gas migration channel. J Biol Chem 2016;291:9052–9. https://doi.org/10.1074/jbc.M115.709154.

- [47] Knapp MJ, Seebeck FP, Klinman JP. Steric control of oxygenation regiochemistry in soybean lipoxygenase-1. J Am Chem Soc 2001;123:2931–2. https://doi.org/ 10.1021/ia003855k
- [48] Vogel R, Jansen C, Roffeis J, Reddanna P, Forsell P, Claesson HE, et al. Applicability of the triad concept for the positional specificity of mammalian lipoxygenases. J Biol Chem 2010;285:5369–76. https://doi.org/10.1074/JBC. M100.057802
- [49] Sloane DL, Leung R, Sigal Cralk CS. E. A primary determinant for lipoxygenase positional specificity. Nature 1991;354:149. https://doi.org/10.1038/354149a0.
- [50] Borngräber S, Kuban RJ, Anton M, Kühn H. Phenylalanine 353 is a primary determinant for the positional specificity of mammalian 15-lipoxygenases. J Mol Biol 1996;264:1145–53. https://doi.org/10.1006/jmbi.1996.0702.
- [51] Borngräber S, Browner M, Gillmor S, Gerth C, Anton M, Fletterick R, et al. Shape and specificity in mammalian 15-lipoxygenase active site. Funct Inter Seq determinants React Specif J Biol Chem 1999;274:37345–50. https://doi.org/ 10.1074/JBC.274.52.37345.
- [52] Bradford MM. A rapid and sensitive method for the quantitation of microgram quantities of protein utilizing the principle of protein-dye binding. Anal Biochem 1976;72:248–54
- [53] Westphal AH, van Berkel WJH. Techniques for Enzyme Purification. In: de Gonzalo G, Lavandera I, editors. Biocatalysis for practitioners: techniques, reactions and applications. 1st ed. Weinheim: Wiley-VCH; 2021. p. 3–31. https://doi.org/10.1002/9783527824465.chl.
- [54] Axelrod B, Cheesbrough TM, Laakso S. Lipoxygenase from soybeans: EC 1.13.11.12 Linoleate: oxygen oxidoreductase. Methods Enzym 1981;71:441–51. https://doi. org/10.1016/0076-6879(81)71055-3.
- [55] Chrisnasari R, Ewing TA, Hilgers R, van Berkel WJH, Vincken J-P, Hennebelle M. Versatile ferrous oxidation-xylenol orange assay for high-throughput screening of lipoxygenase activity. Appl Microbiol Biotechnol 2024;108:266. https://doi.org/10.1007/s00253-024-13095-5.
- [56] Corongiu FP, Bani S. Detection of conjugated dienes by second derivative ultraviolet spectrophotometry. Methods Enzym 1941;233:303–10. https://doi.org/ 10.1016/s0076-6879(94)33033-6.
- [57] Derogis PBMC, Chaves-Fillho AB, Miyamoto S. Characterization of hydroxy and hydroperoxy polyunsaturated fatty acids by mass spectrometry. Adv Exp Med Biol, 1127. Springer New York LLC; 2019. p. 21–35. https://doi.org/10.1007/978-3-030-11488-6 2.
- [58] Derogis PBMC, Freitas FP, Marques ASF, Cunha D, Appolinário PP. The development of a specific and sensitive LC-MS- based method for the detection and quantification of hydroperoxy- and hydroxydocosahexaenoic acids as a tool for lipidomic analysis. PLoS One 2013;8:77561. https://doi.org/10.1371/journal. pone.0077561.
- [59] Jumper J, Evans R, Pritzel A, Green T, Figurnov M, Ronneberger O, et al. Highly accurate protein structure prediction with AlphaFold. Nature 2021;596:583–9. https://doi.org/10.1038/S41586-021-03819-2.
- [60] Hamberg M. Decomposition of unsaturated fatty acid hydroperoxides by hemoglobin: structures of major products of 13L-hydroperoxy-9,11octadecadienoic acid. Lipids 1974;10:87–92. https://doi.org/10.1007/ BF02532161.
- [61] Jin J, Boeglin WE, Cha JK, Brash AR. 8R-Lipoxygenase-catalyzed synthesis of a prominent cis-epoxyalcohol from dihomo-y-linolenic acid: A distinctive transformation compared with S-lipoxygenases. J Lipid Res 2012;53:292–9. https://doi.org/10.1194/ilr.M022863.
- [62] Manivarma T, Nowak W, Tyurina YY, Tyurin VA, Bayir H, Kagan VE, et al. The presence of substrate warrants oxygen access tunnels toward the catalytic site of lipoxygenases. Redox Biol 2025;83. https://doi.org/10.1016/j. redox.2025.103636.
- [63] Shang W, Ivanov I, Svergun DI, Borbulevych OY, Aleem AM, Stehling S, et al. Probing dimerization and structural flexibility of mammalian lipoxygenases by

- small-angle X-ray scattering. J Mol Biol 2011;409:654–68. https://doi.org/ 10.1016/j.imb.2011.04.035.
- [64] Eek P, Poldemaa K, Kasvandik S, Järving I, Samel N. A PDZ-like domain mediates the dimerization of 11R-lipoxygenase. Biochim Biophys Acta Mol Cell Biol Lipids 2017;1862:1121–8. https://doi.org/10.1016/j.bbalip.2017.07.012.
- [65] Mobbs JI, Black KA, Tran M, Burger WAC, Venugopal H, Holman TR, et al. Cryo-EM structures of human arachidonate 12S-lipoxygenase bound to endogenous and exogenous inhibitors. Blood 2023;142:1233–42. https://doi.org/10.1182/BLOOD.2023020441.
- [66] Häfner A-K, Cernescu M, Hofmann B, Ermisch M, Hörnig M, Metzner J, et al. Dimerization of human 5-lipoxygenase. Biol Chem 2011. https://doi.org/10.1515/bc-2011-200
- [67] Pakhomova S, Boeglin WE, Neau DB, Bartlett SG, Brash AR, Newcomer ME. An ensemble of lipoxygenase structures reveals novel conformations of the Fe coordination sphere. Protein Sci 2019;28:920–7. https://doi.org/10.1002/ pro 3602
- [68] Su C, Oliw EH. Manganese lipoxygenase. Purification and characterization. J Biol Chem 1998;273:13072–9. https://doi.org/10.1074/jbc.273.21.13072.
- [69] Brodhun F, Cristobal-Sarramian A, Zabel S, Newie J, Hamberg M, Feussner I. An iron 13S-lipoxygenase with an α-linolenic acid specific hydroperoxidase activity from Fusarium oxysporum. PLoS One 2013;8:e64919. https://doi.org/10.1371/ JOJENSAL PONE 0064919
- [70] An JU, Kim BJ, Hong SH, Oh DK. Characterization of an omega-6 linoleate lipoxygenase from *Burkholderia thailandensis* and its application in the production of 13-hydroxyoctadecadienoic acid. Appl Microbiol Biotechnol 2015;99:5487–97. https://doi.org/10.1007/s00253-014-6353-8.
- [71] Andreou A, Göbel C, Hamberg M, Feussner I. A bisallylic mini-lipoxygenase from Cyanobacterium Cyanothece sp. that has an iron as cofactor. J Biol Chem 2010;285: 14178–86. https://doi.org/10.1074/jbc.M109.094771.
- [72] Deschamps JD, Ogunsola AF, Jameson JB, Yasgar A, Flitter BA, Freedman CJ, et al. Biochemical and cellular characterization and Inhibitor discovery of *Pseudomonas aeruginosa* 15-lipoxygenase. Biochemistry 2016;55:3329–40. https://doi.org/10.1021/acs.biochem.6b00338.
- [73] Zehnder A, Gorham P. R. Factors influencing the growth of Microcystis aeruginosa. Can J Microbiol 1960;6:645–60. https://doi.org/10.1139/m60-077.
- [74] Lehnert N, Solomon EI. Density-functional investigation on the mechanism of Hatom abstraction by lipoxygenase. J Biol Inorg Chem 2003;8:294–305. https://doi. org/10.1007/S00775-002-0415-6.
- [75] Hamberg M, Samuelsson B. On the specificity of the oxygenation of unsaturated fatty acids catalyzed by soybean lipoxidase. J Biol Chem 1967;242:5329–35. https://doi.org/10.1016/S0021-9258(18)99432-9.
- [76] Egmond MR, Vliegenthart JFG, Boldingh J. Stereospecificity of the hydrogen abstraction at carbon atom n-8 in the oxygenation of linoleic acid by lipoxygenases from corn germs and soya beans. Biochem Biophys Res Commun 1972;48: 1055–60. https://doi.org/10.1016/0006-291X(72)90815-7.
- [77] Chrisnasari R, Hilgers R, Li G, Vincken J-P, van Berkel WJH, Hennebelle M, et al. Modulating dioxygenase and hydroperoxide isomerase activities in *Burkholderia thailandensis* lipoxygenase. Enzym Micro Technol 2025;191:110709. https://doi.org/10.1016/J.ENZMICTEC.2025.110709.
- [78] Van Os CPA, Rijke-Schilder GPM, Van Halbeek H, Verhagen J, Vliegenthart JFG. Double dioxygenation of arachidonic acid by soybean lipoxygenase-1 kinetics and regio-stereo specificities of the reaction steps. Biochim Et Biophys Acta Lipids Lipid Metab 1981;663:177–93. https://doi.org/10.1016/0005-2760(81)90204-6.
 [79] Donovan DH, Menzel DB. Mechanisms of lipid peroxidation: Iron catalyzed
- decomposition of fatty acid hydroperoxides as the basis of hydrocarbon evolution in vivo. Experentia 1978;34:775–6. https://doi.org/10.1007/BF01947320.
- [80] Gardner HW. Decomposition of linoleic acid hydroperoxides. Enzymic reactions compared with nonenzymic. J Agr Food Chem 1975;23:129–35. https://doi.org/ 10.1021/jf60198a012.